The Molecular Mechanism of Polymer Formation of Farnesylated Human Guanylate-binding Protein 1

Linda Sistemich [1], Miriam Kutsch [2], Benjamin Hämisch [3], Ping Zhang [1], Sergii Shydlovskyi [1], Nathalie Britzen-Laurent [4], Michael Stürzl [4], Klaus Huber [3] and Christian Herrmann [1]

*1 - **Physical Chemistry I,** Ruhr-University Bochum, 44780, Bochum, Germany*
*2 - **Department of Molecular Genetics and Microbiology,** Duke University Medical Center, Durham, NC27710, USA*
*3 - **Chemistry Department,** University of Paderborn, 33098, Paderborn, Germany*
*4 - **Division of Molecular and Experimental Surgery,** Translational Research Center, Department of Surgery, University Medical Center Erlangen, Friedrich-Alexander University Erlangen-Nürnberg, 91054, Erlangen, Germany*

***Correspondence to Christian Herrmann:** chr.herrmann@rub.de*
https://doi.org/10.1016/j.jmb.2020.02.009
Edited by Bert Poolman

Abstract

The human guanylate-binding protein 1 (hGBP1) belongs to the dynamin superfamily proteins and represents a key player in the innate immune response. Farnesylation at the C-terminus is required for hGBP1's activity against microbial pathogens, as well as for its antiproliferative and antitumor activity. The farnesylated hGBP1 ($hGBP1_{fn}$) retains many characteristics of the extensively studied nonfarnesylated protein and gains additional abilities like binding to lipid membranes and formation of $hGBP1_{fn}$ polymers. These polymers are believed to serve as a protein depot, making the enzyme immediately available to fight the invasion of intracellular pathogens. Here we study the molecular mechanism of hGBP1 polymer formation as it is a crucial state of this enzyme, allowing for a rapid response demanded by the biological function. We employ Förster resonance energy transfer in order to trace intra and intermolecular distance changes of protein domains. Light scattering techniques yield deep insights into the changes in size and shape. The GTP hydrolysis driven cycling between a closed, farnesyl moiety hidden state and an opened, farnesyl moiety exposed state represents the first phase, preparing the molecule for polymerization. Within the second phase of polymer growth, opened hGBP1 molecules can be incorporated in the growing polymer where the opened structure is stabilized, similar to a surfactant molecule in a micelle, pointing the farnesyl moieties into the hydrophobic center and positioning the head groups at the periphery of the polymer. We contribute the molecular mechanism of polymer formation, paving the ground for a detailed understanding of hGBP1 function.
© 2020 The Authors. Published by Elsevier Ltd. This is an open access article under the CC BY license (http://creativecommons.org/licenses/by/4.0/).

Introduction

Guanylate-binding proteins (GBPs) belong to the dynamin superfamily of large GTPases and are key players in the vertebrate immune response against microbial pathogens [1–8]. Furthermore, GBPs show antitumor and antiproliferative activities [9–11]. GBP-mediated defense against bacterial, viral, and protozoan pathogens ultimately triggers pyroptosis [12,13], apoptosis [14], or some other unspecified form of cell death [15,16]. Although the molecular mechanisms underlying GBP-mediated host defense remain poorly understood, it is well known that in order to execute their antimicrobial functions, GBP often requires both associations with cellular and microbial membranes and the ability to form GTP-dependent dimers or higher ordered structures [17–24]. Membrane association of several GBPs is achieved by isoprenylation of the proteins' CaaX box at their C-terminus [25–27]. Self-assembly into dimers and higher ordered structures, as well as GTP hydrolysis, is best characterized for the most prominent isoform of the seven human GBPs (hGBPs), hGBP1. Biochemical

0022-2836/© 2020 The Authors. Published by Elsevier Ltd. This is an open access article under the CC BY license (http://creativecommons.org/licenses/by/4.0/).

studies revealed that hGBP1 is unique in its catalytic mechanism, i.e., it hydrolyzes GTP in a cooperative manner not only to yield GDP but in a subsequent step GMP as the major product [28–30].

The x-ray structure shows hGBP1 to consist of an N-terminal, globular, large GTPase-domain (LG domain) and a C-terminal, purely helical domain, which is subdivided in the middle domain (MD) and the GTPase effector domain (GED) (Fig. 1 A). The MD stretches away from the LG domain in two three-helix bundles (α7-11), and the GED, formed by two helices (α12-13), folds back to the LG domain [31,32]. Positively and negatively charged side chains located in the LG domain and the GED, respectively, form salt bridges mediating tight intramolecular interactions, which result in a closed conformation of the hGBP1 molecule with low GTP hydrolysis activity [29,33,34]. Upon GTP-binding, hGBP1 dimerizes via an LG:LG domain interface, and this intermolecular interaction leads to conformational changes with the following consequences: (1) a catalytic arginine residue is repositioned into the nucleotide-binding site resulting in an increased GTPase activity [29], and (2) the salt bridges between the LG domain and the GED are disrupted resulting in intramolecular structural rearrangements in which the GED moves against the rest of the protein [33,34]. This open conformation leads to increased GMP production [33,35–37]. In contrast to the polymerization of farnesylated hGBP1, which needs active GTP turnover, the association to artificial membranes requires only the binding of GTP [38,39]. We revealed in our previous work that the farnesyl moiety, which is attached to the GED's C-terminus, becomes accessible upon GTP binding and hypothesizes that in the nucleotide-free state of hGBP1 the farnesyl moiety is located in a protein binding pocket. This hypothesis was recently confirmed by a crystal structure of farnesylated hGBP1, which shows the farnesyl moiety accommodated in a hydrophobic pocket, built by residues located in the MD and GED [40].

Polymer formation in the absence of lipids has been observed for other members of the dynamin superfamily, such as dynamin itself, MxA, MxB, Vps1, dnmA, Irga6, and Drp1 [41,42]. Whereas most of the dynamin superfamily proteins (DSP) mediate their function of membrane fission or fusion by polymerizing on and around membranes [42], the biological function of hGBP1 polymers is not revealed yet. Studies of murine GBPs (mGBPs) suggest that GBPs assemble to supramolecular complexes on vesicle-like structures, which attack the vacuole of the protozoan pathogen *Toxoplasma gondii* [23,24]. Also, in uninfected cells, mGBP2 and its human ortholog hGBP1 appear as vesicle-like or granular structures within the cytosol [27,43]. However, hGBP1 is not permanently membrane-associated within the cell, but in a dynamic exchange with the cytosol [39]. Therefore, a part of these vesicle-like or granular structures can be interpreted as a cytosolic pool of hGBP1 polymers. Similar to polymers of the DSP Mx proteins and Drp1 [44–46], hGBP1 polymers might serve as protein depots for rapid mobilization of the protein during the innate immune response or might build the scaffold for inflammasome assembly [4,39,47,48]. Thus, the formation of hGBP1 polymers is an essential feature of this enzyme crucial to understand the antimicrobial function of hGBP1. We use various fluorescence labels, light scattering, enzymology, as well as fluorescence microscopy, in order to address kinetic and structural aspects of hGBP1 polymerization. The results allow us to suggest a detailed model for the molecular mechanism of polymerization.

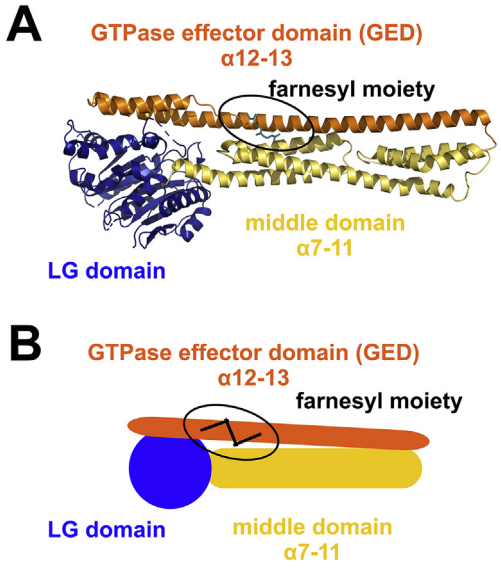

Fig. 1. Domain architecture of the farnesylated human guanylate-binding protein 1 ($hGBP1_{fn}$). (A) Crystal structure of the nucleotide-free $hGBP1_{fn}$ (Protein Data Bank ID code: 6K1Z). The protein consists of three domains: The large GTPase domain (LG domain; blue), the helical middle domain (MD; α7-11; yellow), and the helical GTPase effector domain (GED, α12-13; orange) with the attached farnesyl moiety (black; circled). **(B)** Schematic representation of the crystal structure with the different domains colored as in (A).

Results

Polymerization of $hGBP1_{fn}$ is preceded by dimerization and an intramolecular rearrangement of the GED

The farnesylated form of hGBP1 ($hGBP1_{fn}$) shows special features compared with the nonfarnesylated

wild type protein, which is gained by the lipid moiety. We recently demonstrated that $hGBP1_{fn}$ is able to form polymeric structures in a GTP dependent and reversible manner [39]. In our previous work, we monitored polymerization with an absorbance-based turbidity assay and analyzed the accompanying GTP-hydrolysis over time. By this, we could link different rates of GTP hydrolysis to different phases of polymer growth and could attribute the final disassembly of the polymer to GTP depletion [39]. Like in our previous work, we refrained from cleaving off the three C-terminal residues of hGBP1 after enzymatic farnesylation. In the x-ray structure of $hGBP1_{fn}$, the three residues are also present, and they do not show any intramolecular contacts in addition to the farnesyl tail [40].

As the process of polymerization is based on intermolecular interactions, we hypothesized that polymerization could be tracked by our developed intermolecular Förster resonance energy transfer (FRET) assay [37] (see Methods section). Therefore, we mixed equimolar concentrations of acceptor and donor labeled $hGBP1_{fn}$, respectively, and induced interaction by the addition of 1 mM GTP. The course of intermolecular interaction was then monitored by exciting the donor fluorophore (AlexaFluor488) and detecting the emission of the acceptor fluorophore (AlexaFluor647). The profile of the resulting fluorescence time course equals the time course for polymerization assayed by turbidity. Both setups show no signal increase directly after nucleotide addition, and this period is termed phase I (pink). After this lag phase, the absorption/fluorescence rises and decays after time, and this period is termed phase II (green) (SI Fig. S1 A, B). As there is hardly any interference of fluorescence at 664 nm and turbidity (SI Fig. S1 C), the FRET set-up can be employed to follow $hGBP1_{fn}$ polymerization. In addition, photobleaching of the donor and acceptor dye can be excluded since the control

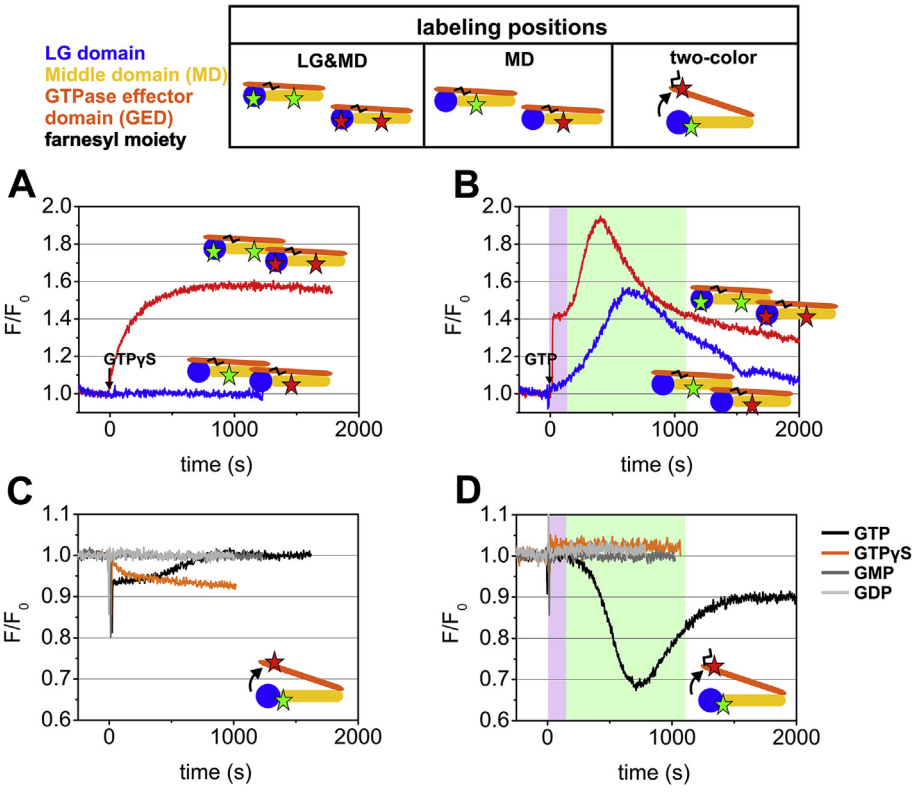

Fig. 2. Inter- and intramolecular distance changes of $hGBP1_{fn}$ domains within the course of polymer formation. **Top**: Overview of the labeling positions in $hGBP1_{fn}$ with the domains highlighted in different colors accordingly to Fig. 1, LG domain blue, MD yellow, GED orange. The farnesyl moiety is depicted as a black zigzag line. AlexaFluor488 is depicted as a green star, and AlexaFluor647 is depicted as a red star, located on the respective domains. **(A,B):** Fluorescence time courses of intermolecular FRET of differently labeled constructs of $hGBP1_{fn}$. Donor labeled and acceptor labeled $hGBP1_{fn}$, respectively, were mixed with an equimolar ratio. Labeling positions are highlighted with a star. Red curve: LG&MD labeled $hGBP1_{fn}$, blue curve: MD labeled $hGBP1_{fn}$, in the presence of 250 μM GTPγS (A) and 1 mM GTP (B), respectively. Area in pink: phase I, area in green: phase II. **(C,D):** Fluorescence time courses of intramolecular FRET of hGBP1 (C) and $hGBP1_{fn}$ (D), respectively, in the presence of different nucleotides (black: GTP, orange: GTPγS, gray: GMP, light gray: GDP).

measurements with monomeric GMP or GDP-bound protein (Fig. 2 C, D) show a stable signal over time.

Next, we wanted to use this FRET set up to investigate the domains of the neighboring $hGBP1_{fn}$ molecules, which interact in the course of polymerization. To this end we generated $hGBP1_{fn}$ variants with defined labeling positions. We were able to guide one fluorescent label to the MD domain only and, by choosing higher concentrations and longer incubation time, to attach two labels to the MD&LG domain as concluded from limited tryptic digestion experiments (SI Fig. S2 C, D). Hence, we had FRET pairs in hand to monitor interactions between MDs and between LG domains, respectively, namely only MD labeled and LG&MD labeled. MD:MD and LG:LG domain interactions were investigated in dependence of GTP and its non-hydrolyzable analog GTPγS to distinguish between interactions induced by GTP-hydrolysis (GTP) and by GTP binding (GTPγS), respectively. The addition of GTPγS to $hGBP1_{fn}$ showed an increase in acceptor fluorescence due to intermolecular FRET only for the FRET pair LG&MD labeled but not for the MD labeled (Fig. 2 A). We concluded that the binding of GTPγS only induces interactions between the LG domains but not between the MDs. This was also reflected in the first seconds of the fluorescence profiles recorded for GTP (Fig. 2 B): directly after GTP addition we observed a sudden increase in acceptor fluorescence for the FRET pair sitting at the LG&MD but not for the FRET pair located at the MDs (phase I, pink). However, after a lag time, the acceptor fluorescence slowly increased for the latter FRET pair matching the onset of polymerization. Simultaneously, an additional slow increase of acceptor fluorescence for the LG&MD labeled FRET pair was observed (Fig. 2 B; phase II, green). The shift of the maximum of polymerization to earlier times for the LG&MD labeled $hGBP1_{fn}$ compared to the MD labeled $hGBP1_{fn}$ can be explained by a small impact of the labels on polymerization, which is also observed when performing turbidity measurements with the different labeled constructs (SI Fig. S1 D).

Our previous studies with nonfarnesylated hGBP1 revealed that during dimerization, the GED rearranges by detachment from the rest of the protein; of course, MD and GED remain covalently linked between α11 and α12. This structural rearrangement we term ‘‘opening,’’ and it is (1) triggered by GTP binding, (2) stabilized during nucleotide hydrolysis, and (3) reverts upon GTP depletion as described for nonfarnesylated hGBP1 [33,36,37,49,50]. Thus, we aimed to monitor structural rearrangements within the $hGBP1_{fn}$ molecule during the polymerization process. Therefore, we employed the intramolecular FRET assay, where both the donor and the acceptor fluorophores are attached to the same hGBP1 molecule [37]. Having the acceptor fluorophore placed at the C-terminus of the GED (for farnesylated hGBP1 at a cysteine introduced at position 577, and for nonfarnesylated hGBP1 at position C589) and the donor fluorophore on the opposite side of the protein (MD or LG) (SI Fig. S2 E,F) allowed us to monitor a change in distance between the GED and the rest of the protein. This two-color-labeled protein was incubated with a 10-fold excess of unlabeled protein of the same kind to minimize intermolecular FRET. Then GTPγS, GTP, GDP, or GMP was added in order to monitor domain rearrangements induced by nucleotide binding, during GTP hydrolysis, and after GTP hydrolysis, respectively. In this assay, an opening or a movement of the GED relative to the rest of the protein is reported by a loss in acceptor fluorescence. As expected, no change in intramolecular FRET was observed upon the addition of GMP or GDP for both hGBP1 and $hGBP1_{fn}$ (Fig. 2 C, D). However, we observed different fluorescence profiles for farnesylated and nonfarnesylated hGBP1 when binding GTP and during GTP-hydrolysis, respectively. The acceptor fluorescence of nonfarnesylated protein hGBP1 dropped instantly after GTP addition, which we interpreted as an immediate movement of the GED or opening of the protein (Fig. 2 C). In contrast, the farnesylated protein opened with slower kinetics after a lag time of 1−2 min (Fig. 2 D; phase I, pink). Both farnesylated and nonfarnesylated hGBP1 remained open for several cycles of GTP turnover. When GTP decayed to low concentrations and finally was completely consumed by the hydrolysis, both proteins showed an increase in acceptor fluorescence suggesting the reclosing of their structure (Fig. 2 C, D and SI Fig. S1 E, F). Of note, the GTP-induced, time-dependent fluorescence profile of intramolecular FRET for the farnesylated protein strongly resembled the profile of polymerization obtained from intermolecular FRET measurements (SI Fig. S1 B, gray curve mirrored on the x-axis). Intriguingly GTP binding alone, probed by the use of GTPγS, was able to shift hGBP1 toward the opened structure but not $hGBP1_{fn}$ (Fig. 2 C and D). This is explained by a contribution from the farnesyl tail to stabilize the closed structure.

Thus, by FRET-based tracking of distance changes between two different LG domains, between two different MDs, and between the GED and the LG/MD of the same molecule, respectively, we were able to demonstrate that (1) in phase I of polymerization the first contact is formed rapidly between the LG domains upon GTP binding, (2) after a lag time the GED moves away from LG/MD, and (3) concomitantly the MDs approach each other in phase II. Note that within phase I (lag phase), the GTP turnover is slow without formation of GMP, while in phase II, the GTP turnover is much faster, and GMP is formed.

LG domain-mediated dimerization is crucial as the first interaction site of polymerization

We noted that the extent of polymerization is dependent on the concentration of $hGBP1_{fn}$. Higher protein concentrations showed a larger absorbance, and thus, more turbidity than smaller protein concentrations. Still, turbidity for $hGBP1_{fn}$ concentrations as small as 0.5 μM was detectable. Moreover, the time courses of absorbance for all

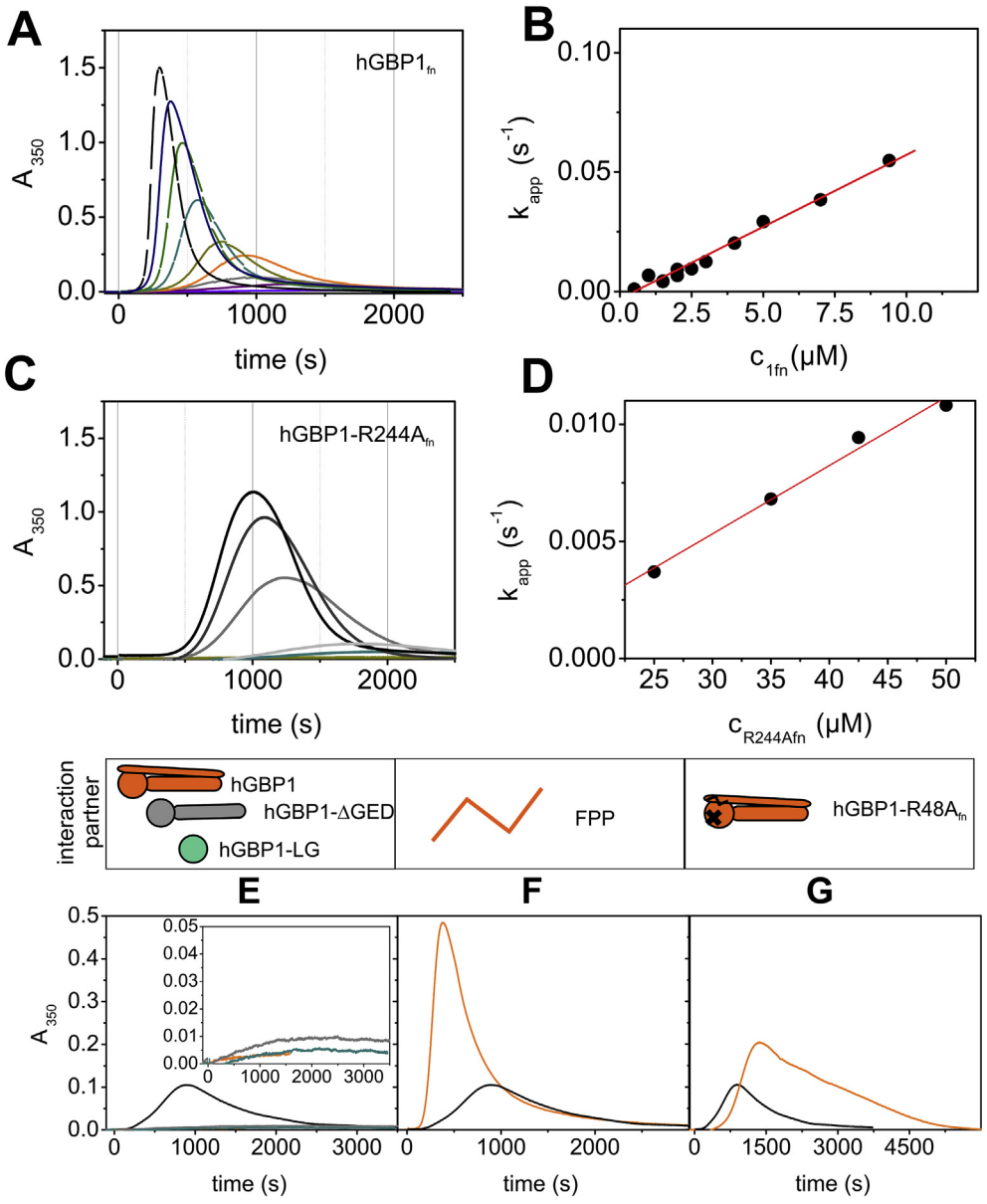

Fig. 3. Polymerization kinetics of wild type and LG:LG contact-weakened mutant $hGBP1\text{-}R244A_{fn}$ and interference of truncated hGBP1 constructs. (A): Concentration-dependent polymerization of $hGBP1_{fn}$ (0,5 μM–9,5 μM) in presence of 1 mM GTP. The absorbance time courses were modeled by Equation (1) (methods section) yielding k_{app} values and lag times for each concentration. **(B):** The linear dependency of k_{app} on the protein concentration revealed the polymer association rate constant for $hGBP1_{fn}$, $k_{ass} = 0.006\ s^{-1}*\mu M^{-1}$. **(C)**: Polymerization of $hGBP1\text{-}R244A_{fn}$ (25–50 μM) in presence of 5 mM GTP. As in (A) the absorbance time courses yielded lag times and k_{app} values. **(D):** The linear dependency of k_{app} on the $hGBP1\text{-}R244A_{fn}$ concentration results in $k_{ass} = 0.0003\ s^{-1}*\mu M^{-1}$. **(E–G):** Absorbance reporting polymerization of 2 μM $hGBP1_{fn}$ in the presence of different interaction partners induced with 1 mM GTP at t = 0 s (black curves: 2 μM $hGBP1_{fn}$ only). **(E):** orange: plus hGBP1 (2 μM), gray: plus hGBP1-ΔGED (2 μM), cyan: plus hGBP1-LG (2 μM). **(F)**: orange: plus farnesyl pyrophosphate, FPP (40 μM) **(G)**: orange: plus $hGBP1\text{-}R48A_{fn}$ (4 μM).

concentrations showed the two characteristic phases, namely the lag time in absorbance accompanied by slow GTP turnover (phase I) and the phase of turbidity increase reporting polymer assembly together with fast GTP hydrolysis (phase II) followed by disassembly once GTP is depleted. The smaller the concentration of $hGBP1_{fn}$ was chosen, the longer the lag time, i.e., the later was the onset of turbidity, and the slower was the rate of the turbidity increase (Fig. 3 A). From the absorbance time courses, we obtained information on the association kinetics of the polymer (SI Fig. S3 A). Lag times, as well as apparent elongation rate constants (k_{app}), were obtained, the latter of which increased with increasing protein concentration (Fig. 3 B), while the lag time decreased with increasing protein concentration (SI Fig. S3 B). The slope of the linear dependency of k_{app} on $hGBP1_{fn}$ concentration was interpreted as the polymer association rate constant, yielding $k_{ass} = 0.0060\ s^{-1}\mu M^{-1}$ (Fig. 3 B). Utilizing the intermolecular FRET-assay to monitor concentration-dependent polymerization revealed almost the same association kinetic with $k_{ass} = 0.0059\ s^{-1}\mu M^{-1}$ (SI Fig. S3 C,D).

In order to address the importance of dimer formation for polymerization, we challenged the LG:LG domains contact site. The arginine at position 244 was previously identified as one of two major determinants (next to R240) of GTP-induced dimerization. We demonstrated that changing the arginine at position 244 to alanine results in a dimer interface-weakened mutant, with the same nucleotide-binding affinities and maximal GTP turnover number as the wild type protein [51]. The weakened dimerization required us to determine the polymerization kinetics of the mutant R244A to be carried out at higher protein concentrations. Also, since the GTP turnover of the mutant is similar to wild type protein, we chose 5 mM GTP instead of 1 mM GTP to prevent early GTP depletion. The dimerization interface-weakened mutant $hGBP1\text{-}R244A_{fn}$ showed significant polymerization with a concentration of up to 50 μM, while the wild type polymerizes already at concentrations of 5 μM to the same level (Fig. 3 A, C). This difference in concentration requirements is rationalized by the 10-fold difference of the dimer dissociation constant ($K_{D;\ wild\ type} = 0.3\ \mu M$ and $K_{D;\ R244A} = 3.1\ \mu M$) [51]. For $hGBP1\text{-}R244A_{fn}$, the resulting polymer formation rate constant (Fig. 3 D, $k_{ass} = 0{,}0003\ s^{-1}*\mu M^{-1}$) is smaller by a factor of 20 compared to the wild type. A further difference between mutant and wild type is that the lag phase is prolonged for the dimerization interface weakened mutant (Fig. 3 A, C). These differences in the process of polymer formation allowed us to conclude that interaction via the LG domains is central for the process of polymerization.

Polymer formation responds sensitively to the presence of nonfarnesylated or truncated hGBP1

Our previous study has revealed that farnesylation of hGBP1 is mandatory for polymerization, i.e., $hGBP1_{fn}$ forms polymers after GTP addition in contrast to nonfarnesylated hGBP1 [39]. So far, we had shown that LG domains and MDs, respectively, approach each other during polymerization. Next, we wanted to know if these domains are required for polymer formation. We hypothesized that hGBP1 variants lacking one of the interaction sites would fail to be incorporated into the polymer. In order to test this hypothesis, we employed the turbidity assay, where $hGBP1_{fn}$ was incubated with different variants of hGBP1 as potential copolymerization partners at defined concentrations and polymerization was triggered by the addition of GTP. During the course of the polymerization, the nucleotide composition was quantified by HPLC analysis in order to compare the GTP hydrolysis rates in the different phases.

Knowing that the farnesyl moiety is crucial for polymerization [39] and having shown that in phase I LG:LG contacts are established (Fig. 2 B), we started to define copolymerization partners by shortening $hGBP1_{fn}$ from the C-terminus. Firstly, the farnesyl moiety was removed, resulting in the nonfarnesylated wild type protein (hGBP1). Secondly, α12/13 representing the GED were truncated, resulting in the loss of the helical interaction site at the C-terminus but preserving the LG:LG domain and MD:MD interaction sites (hGBP1-ΔGED). And third, the MD was removed in addition, yielding the isolated LG domain without any helical domain (hGBP1-LG). As expected, none of the interaction partners on its own showed the ability to polymerize after the addition of GTP. For addressing potential copolymerization, each of the three hGBP1 variants was added in equimolar amounts (2 μM each to 2 μM $hGBP1_{fn}$), and polymerization was triggered by the addition of GTP. The turbidity assay showed an almost complete abolishment of polymer formation in all three experiments (Fig. 3 E). We concluded that the truncated variants failed to be incorporated into the polymer and suggested that the impairment of polymerization was due to mixed dimer formation. Only homodimers of $hGBP1_{fn}$ can build polymers while heterodimers like $hGBP1_{fn}$:hGBP1 cannot. Already small amounts of each of the three truncated hGBP1 variants (1 μM to 10 μM of $hGBP1_{fn}$) showed an impairment of $hGBP1_{fn}$ polymerization, the more the interacting hGBP1 was truncated: Nonfarnesylated hGBP1 brought the absorbance down by a factor of 2 and hGBP1-ΔGED, as well as hGBP1-LG, decreased the absorbance even by a factor of 6 (SI Fig. S4 A). With the addition of hGBP1-ΔGED and

hGBP1-LG, respectively, the lag phase of polymerization was preserved while GTP was hydrolyzed rapidly from the beginning due to the high activity of nonfarnesylated hGBP1 variants (SI Fig. S4 A, D).

Addressing the importance of the farnesyl moiety from the other side, i.e., by the addition of an excess of farnesyl pyrophosphate (40 μM FPP to 2 μM $hGBP1_{fn}$), we observed a shortened lag phase of polymerization and an increase of the turbidity maximum (Fig. 3 F). The pronounced and premature polymerization driven by FPP was also observed when monitoring the intramolecular opening of $hGBP1_{fn}$ in the presence of FPP, showing a shorter lag phase and even less acceptor fluorescence (SI Fig. S4 G). In addition, the turnover number was increased by a factor of 1.4 in the presence of FPP compared with $hGBP1_{fn}$ alone (SI Fig. S4 E). Based on these observations, we concluded that the hydrophobic interactions of the farnesyl moieties enhance the polymerization of hGBP1, most likely, due to the stabilization of the protein's outstretched conformation and due to the increased overall farnesyl concentration favoring the formation of the micelle-like, hydrophobic core.

The ability of $hGBP1_{fn}$ to catalyze GTP hydrolysis has to be considered. The mutant hGBP1-R48A, lacking the catalytic arginine at position 48, is able to bind GTP with the same affinity as the wild type protein but is 100 times slower in GTP hydrolysis [52]. While the farnesylated mutant hGBP1-$R48A_{fn}$, on its own, is not capable of polymerizing [39], the addition of this farnesylated mutant (4 μM) to $hGBP1_{fn}$ (2 μM) did not interfere with polymerization, which is in contrast to the truncated variants described above. The maximum of turbidity of $hGBP1_{fn}$ is increased in the presence of hGBP1-$R48A_{fn}$, the onset of turbidity is delayed, and polymerization is prolonged (Fig. 3 G). The same effects are observed when monitoring the intramolecular opening of $hGBP1_{fn}$ in the presence of hGBP1-$R48A_{fn}$ (SI Fig. S4 H). Measurements of GTPase activity revealed in phase II, a slightly lower hydrolysis rate compared to $hGBP1_{fn}$ alone (SI Fig. S4 C, F). Based on these observations we hypothesized that other than the truncated hGBP1 variants, the hydrolysis-deficient mutant can be incorporated into the polymer as it offers all interaction sites that are needed and as it only slightly reduces the hydrolysis activity of $hGBP1_{fn}$. Incorporation of hGBP1-$R48A_{fn}$ is furthermore confirmed by performing concentration-dependent intermolecular FRET-measurements with equimolar amounts of donor labeled hGBP1-$R48A_{fn}$ and acceptor labeled $hGBP1_{fn}$ to reveal an association rate constant k_{ass} of 0.00134 $s^{-1}\mu M^{-1}$ (SI Fig. S4 J, K).

In summarizing the observations, the farnesyl moiety is not only important for polymerization, but a small fraction of nonfarnesylated hGBP1 also impairs the polymerization of $hGBP1_{fn}$. This impairment is even more pronounced in the presence of a small fraction of hGBP1-ΔGED. Together with the conclusions from the previous chapter, we suggest a coparallel arrangement of the $hGBP1_{fn}$ molecules in the polymer resulting in the stabilization of an outstretched protein.

Facilitated opening favors polymer formation

In the nucleotide-free state, $hGBP1_{fn}$ shows a compact structure, and the farnesyl moiety is suggested to strengthen the contact between GED and LG/MD by residing in a hydrophobic protein pocket [40]. In the course of the polymerization, the protein changes its conformation by opening, and it ends up fully outstretched in the polymer as we concluded from negative stain EM data [39] and as supported by our observations described above. As we could see with the aid of the intramolecular FRET assay (Fig. 2 D), the shift of the equilibrium toward the open conformation takes some time, and this process coincides with the first phase of polymerization and slow GTP hydrolysis. Beforehand most of the protein population remains closed. Thus, a hGBP1 mutant with a weakened contact between LG domain and GED will be suitable in order to test if the first phase of polymerization is a process of establishing and stabilizing the opened and finally the outstretched conformation. We hypothesized that a constitutively open hGBP1 mutant should facilitate establishing the outstretched protein. The double mutant hGBP1-R227E/K228E (termed hGBP1-RK) lacks the electrostatic interaction between the α4′-helix in the LG domain and the GED due to charge reversal [33], leading to a facilitated opening. This feature is still preserved after the farnesylation of the protein, as we demonstrated by intramolecular FRET measurements (Fig. S5 A). In the time course of the polymerization, we observed that hGBP1-RK_{fn} lacks the first phase of polymerization (Fig. 4 A), where wild type turbidity is not detectable, and GTP is only slowly hydrolyzed (Fig. 4 B). Immediately after addition of GTP to hGBP1-RK_{fn}, all characteristics of phase II (Fig. 4, marked in green) of polymerization were observable: the polymer instantly started growing, reflected by an immediate increase of absorbance, and GTP was turned over immediately with high catalytic activity. Notably, the extent of polymer formation of hGBP1-RK_{fn} was decreased compared to the wild type protein. This was reflected by an 8 × times smaller absorbance maximum and depolymerizing within half of the time compared to $hGBP1_{fn}$ (Fig. 4 A, B). Smaller turbidity of hGBP1-RK_{fn} due to much earlier depletion of GTP (Fig. 4 A, B) tracking the nucleotide amounts of GTP, GDP, and GMP) is observed for two reasons: the GTPase activity is 2−3 times higher and, noteworthy the lag phase in GTPase activity is completely missing for the RK_{fn} mutant whereas wild

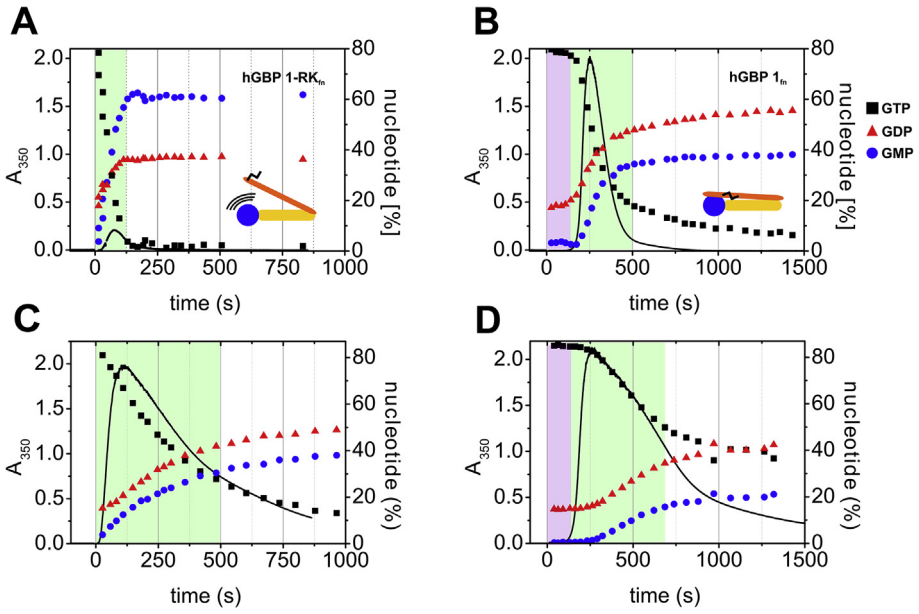

Fig. 4. Opening and polymer formation of the LG:GED contact-weakened mutant hGBP1-RK$_{fn}$. (A–D): Absorbance time course of polymerization at 10 μM each of the open mutant hGBP1-RK$_{fn}$ (A,C) and hGBP1$_{fn}$ (B,D) after injection of 1 mM GTP (A,B) and 5 mM GTP (C,D), respectively, superimposed by the time course of nucleotide composition in the same solution (black: GTP, red: GDP, blue: GMP, phase I: pink, phase II: green).

type shows slow GTP hydrolysis for the initial 2–3 min. Having demonstrated, that depolymerization takes place when GTP is completely turned over by hGBP1, we asked, if we obtain a higher extent of polymerization—characterized by higher absorbance values and/or longer polymerization times—when providing more substrate. And indeed, when offering a 5 × times higher amount of GTP the persistence of the RK$_{fn}$ mutant and wild type polymerization was prolonged 3 × times to 4 × times (Fig. 4 C, D). Changes due to higher GTP concentration were even more distinct for the hGBP1-RK$_{fn}$ mutant. While hGBP1$_{fn}$ showed no significant increase of turbidity with 5 mM GTP, for hGBP1-RK$_{fn}$, an increase of the maximum of absorbance by a factor of 10 was observed, reaching the level of wild type. Nevertheless, the lag phase (phase I) of polymerization and of GTPase activity was not detectable for hGBP1-RK$_{fn}$, and it instantly showed polymer formation after GTP addition. Also, the intramolecular FRET data support a facilitated, instantaneous opening of hGBP1-RK$_{fn}$. In contrast to the wild type, which shows a delay (see Fig. 2 D), for hGBP1-RK$_{fn}$, an immediate drop of the FRET efficiency is observed (SI Fig. S5 A). Noteworthy, this drop in FRET is not as pronounced, as for wild type (compare Fig. 2 D and SI Fig. S5 A), suggesting an equilibrium of opened and closed structure for hGBP1-RK$_{fn}$ without nucleotide while the farnesylated wild type resides only in the closed population before GTP is added.

To further address the relationship of opening and polymerization, we used the transition state analog GDP*AlF$_x$. In our previous study, we interpreted the EM structure of the hGBP1$_{fn}$ polymer in the presence of GDP*AlF$_x$ as one or a few circular layers of the molecule based on the coincidence of their radius and the length of the hGBP1$_{fn}$ molecule completely stretched out [39]. Using the established assay for intramolecular FRET [37] (see Methods section) we observed, that GDP*AlF$_x$ opens the conformation of hGBP1$_{fn}$ in a nonreversible manner (SI Fig. S5 B). A permanently outstretched conformation is even detectable for the farnesylated hGBP1-RK mutant in the presence of GTPγS and GppNHp, respectively, which can be attributed to the facilitated opening for the RK mutant (SI Fig. S5 A). We checked by dynamic light scattering analysis if these nucleotides lead to polymer formation of hGBP1-RK$_{fn}$ as observed for the wild type protein in the presence of GDP*AlF$_x$. First, the nucleotide-free states of nonfarnesylated and farnesylated hGBP1 and hGBP1-RK, respectively, were examined. Within the error limits of the instrumentation (HPPS-High Performance Particle Sizer, Malvern) and data analysis, no significant difference was found between the four experiments. The presence of the nonhydrolyzable analogs, GTPγS, as well as GppNHp, led to a shift toward larger radii (SI Fig. S5 C). In the case of hGBP1 and nonfarnesylated double mutant, this is accounted for by the establishment of a monomer/dimer equilibrium. In contrast, the farnesylated RK mutant showed diameters close

to 50 nm suggesting polymer formation and again, supporting the notion that opening and polymerization is facilitated by this double mutation (Fig. S5 C). For GDP*AlF$_x$-bound hGBP1 we had already shown that the equilibrium for the nonfarnesylated protein [37] is shifted, presumably, completely to the dimer population as confirmed here, and the same was observed for the double mutant (SI Fig. S5 C). The farnesylated wild type, as well as the double mutant form polymers, when bound to GDP*AlF$_x$ and DLS revealed a similar, large diameter of almost 50 nm, which is in good agreement with the value observed with EM for the circular structures previously [39]. Nevertheless, neither the GTP-analogs GTPγS, GppNHp nor the GTP transitions state analog GDP*AlF$_x$ induced polymerization in the same way and to the same extent as GTP did (SI Fig. S5 D).

To summarize, polymerization is enabled by GTPase activity driven opening of hGBP1$_{fn}$. This can be mimicked by the transition state analog GDP*AlF$_x$, at least, leading to the formation of small polymers. In the case of the intrinsically opened RK mutant, a nonhydrolyzable analog-like GTPγS responsible for LG:LG contact formation is sufficient. This means that the opening is required for polymerization. As characteristic differences in polymerization behavior became evident between GTP and GDP*AlF$_x$, we may further hypothesize the relevance of dynamic changes in hGBP1 structures due to the cycling through GMP-, GDP- and GTP bound states as opposed to the kind of static situation in the hGBP1$_{fn}$-GDP*AlF$_x$ complex.

GTP induced hGBP1 polymer formation is distinguished by the continuous addition of hGBP1$_{fn}$ units

We wanted to explore further the mechanism of polymer formation and therefore employed time-dependent dynamic and static light scattering, which

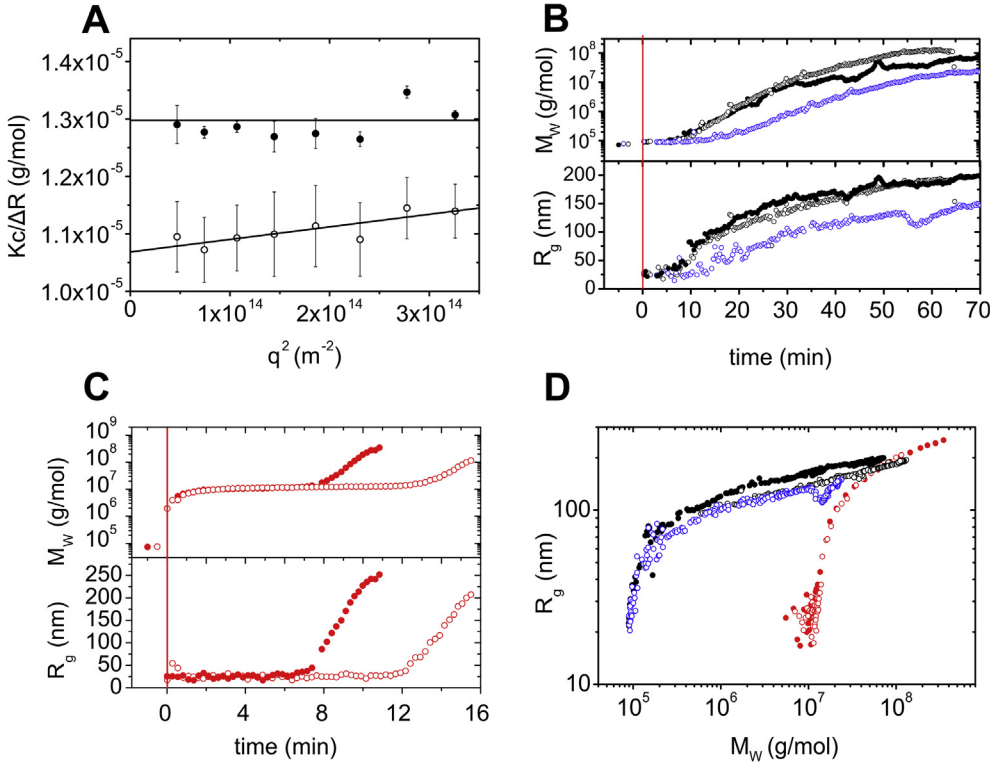

Fig. 5. Analysis of hGBP1$_{fn}$ polymerization by static and dynamic light scattering. (A): Zimm-plots of time averages revealing the molecular weight of hGBP1$_{fn}$ before (filled circle) (M_W = 77,000 g/mol) and after (open circle) addition of GTP (M_W = 93,600 g/mol). The data after addition of 1 mM GTP are based on a time average covering the first 6 min after addition of GTP at 15 °C. The concentration of hGBP1$_{fn}$ is 10 μM. **(B):** Polymerization of 10 μM (black filled and open circle) and 5 μM (blue open circle) hGBP1$_{fn}$ induced by the addition of 1 mM GTP at 15 °C. Evolution of the molar mass (upper panel) and the radius of gyration (lower panel). **(C):** Polymerization of 10 μM hGBP1$_{fn}$ at 25 °C induced by the addition of 250 μM GDP*AlF$_x$. Evolution of the molar mass (upper panel) and the radius of gyration R_g (lower panel). The two symbols represent two runs performed under identical conditions. **(D):** Correlation of the size in terms of the radius of gyration with the corresponding weight average molar mass of the growing particles, both from SLS. The symbols have the same meaning as in panels B and C.

enabled us to record time courses of polymerization and to characterize the appearance of the formed polymers in terms of size, shape, and number of incorporated proteins.

SLS data yielding the weight averaged mass of the proteins in solution showed an immediate increase from $0.7 \cdot 10^5$ g/mol to $1.0 \cdot 10^5$ g/mol after GTP addition (Fig. 5 A, B). This supports the notion of the establishment of a monomer/dimer equilibrium in the GTP bound state. Given this equilibrium, a weight averaged molar mass of $1.0 \cdot 10^5$ g/mol corresponds to 30%, 22%, and 18% by weight of the dimer fraction for the three experiments carried out (Fig. 5 A, B), respectively.

Obviously, the time of partial dimerization coincided with the lag phase described above and termed phase I. Then, the average mass starts to increase further, and a more or less steady growth up to 10^8 g/l is observed within 50 min (Fig. 5 B). This polymerization leads to the size of 100 $hGBP1_{fn}$ molecules per polymer after 30 min, growing steadily further to 1000 molecules per polymer or more.

In order to learn more about the shape of the polymers, the ratio ρ of the radius of gyration R_g and the hydrodynamic radius R_h of the growing polymer was determined to serve as a shape-sensitive parameter (SI Fig. S6 A). For the GTP-induced polymer, this shape-sensitive ratio ρ equals 0.7 over

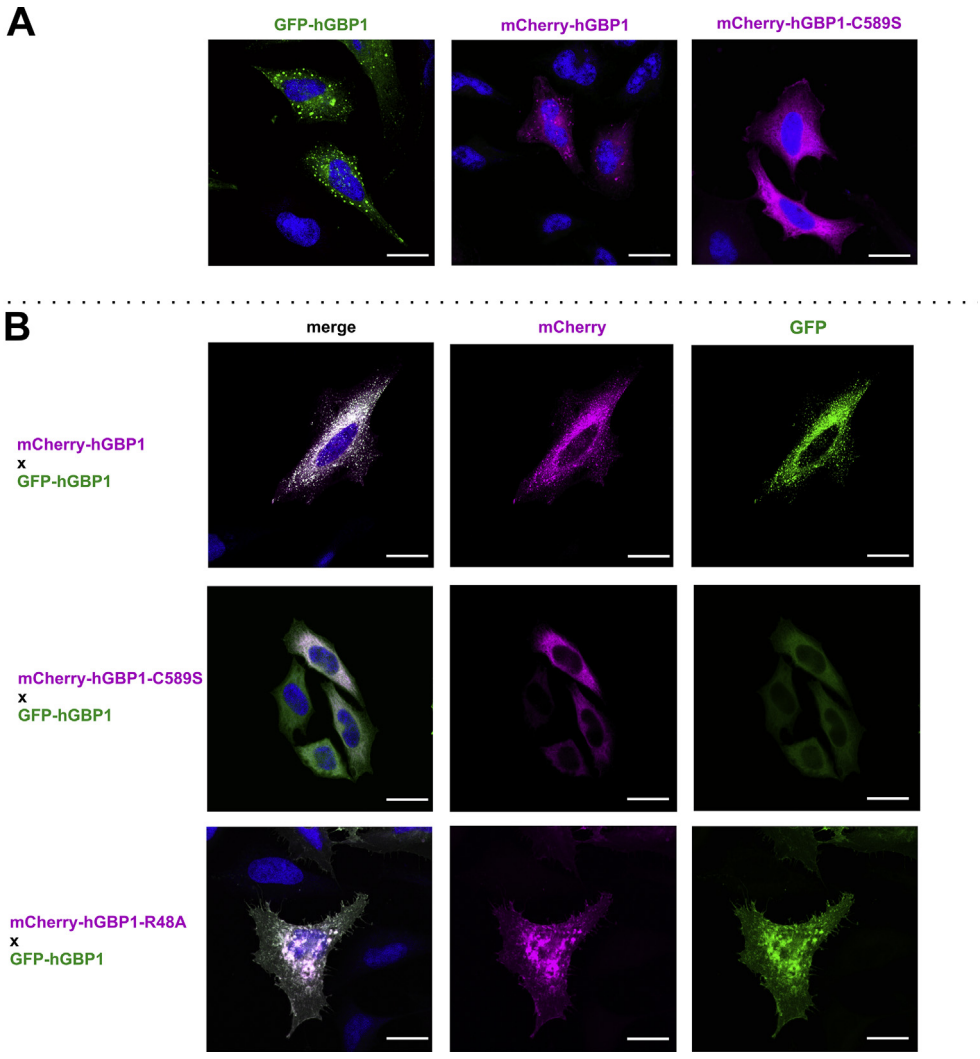

Fig. 6. Localization in HeLa cells that were transfected with plasmids encoding GFP and mCherry-tagged hGBP1 and hGBP1-C589S. Nuclei were counterstained with Draq5. **(A):** GFP-hGBP1 and mCherry-hGBP1 is distributed in the cytoplasm with a partly granular structure. mCherry-hGBP1-C589S is distributed homogenously in the cytosol. **(B):** Co-expression of mCherry-hGBP1 and GFP-hGBP1 (upper panel) results in co-localization of both proteins in granular structures in the cytosol. Co-expression of mCherry-hGBP1-C589S and GFP-hGBP1 (middle panel) results in a homogenous cytoplasmic distribution. Coexpression of mCherry-hGBP1-R48A and GFP-hGBP1 (lower panel) results in co-localization of both proteins in large granular structures in the cytosol. Scale bar: 25 μm.

the full-time course, which is compatible with compact structures [53] with a homogenous density.

All time-resolved light scattering experiments carried out with GTP in the presence or the absence of BSA (see methods section: Sample preparation for Static and Dynamic Light Scattering experiments) reveal the same trend, which is after the lag phase the continuous growth of particle mass and size at a constant shape parameter ρ. A closer look on the data from DLS shed light on the polymerization mechanism. The intensity-time correlation functions indicate two well-separated decays (Fig. S6 B), suggesting diffusional modes from two different species. Decomposition of the field-time correlation function with a bimodal decay, revealing an increase of the contribution of the slow mode at the expense of the fast mode (Fig. S6 C, D). Accordingly, the fast mode, can be attributed to the monomers/dimers, which decreases with time, and the slow mode to the growing polymer. The observed loss of the fast mode, which is in line with the rise of the fast mode can be attributed to a growth of the polymer by the addition of monomeric or dimeric protein units. This process describes phase II of polymerization. Coalescence of any two approaching particles according to a step-growth process would reveal a monomodal distribution of decay times throughout the entire process. Finally, it should not be left unmentioned that the dimer shows a relatively large size as the radius of gyration has a value of 20−30 nm suggesting an opened structure (Fig. 5 B, lower panel).

GDP*AlF$_x$ induces formation of polymers without lag phase

A different growth pathway is revealed by time-resolved light scattering for the polymerization in the presence of the transition state analog GDP*AlF$_x$ (Fig. 5 C). After nucleotide addition, polymerization of hGBP1$_{fn}$ occurs immediately without delay. Within 2 min, the weight averaged molar mass value increases by approximately two orders of magnitude to 10^7 g/mol. This is 100−200 fold larger than the monomeric unit, which was defined prior to nucleotide addition with $0.8 \cdot 10^5$ g/mol. Thus, the observed increase in the molecular weight suggests an assembly of 100−200 hGBP1$_{fn}$ molecules. In contrast to the cycling between monomer and dimer species and the delayed polymerization induced by GTP, i.e., phases I and II, polymerization in the presence of GDP*AlF$_x$ occurs instantaneously. This is also supported by FRET experiments. After the addition of GDP*AlF$_x$, the contacts between the LG domains, as well as between MDs, are detected without delay, and the opening as reported by the drop of intramolecular FRET occurs instantaneously as well (SI Fig. S5 B).

In the presence of GDP*AlF$_x$, the radius of gyration R_g measured for the degree of polymerization of 100−200 molecules is close to 25 nm, and thus, similar to the GTP bound dimer mentioned above. The formed polymers remain unchanged in shape and mass for 10 min and thereafter resume growth during a second period with the polymer mass increasing by more than one order of magnitude within 2−3 min. During the first time period, immediately following the addition of GDP*AlF$_x$ the ratio R_g/R_h also remains constant at $\rho = 0.8$, which is similar to the value observed for the intermediates growing in the presence of GTP and which is compatible with spherical [53] or disc-like objects [54]. The plateau is followed by another phase of growth, leading to highly anisometric shapes, since the ratio ρ steeply increases with the onset of further growth (SI Fig. S6 E). During the entire time course of the polymerization, the intensity-time correlation function did not show any bimodal behavior (SI Fig. S6 F). Therefore, we can conclude that the formation of the small polymers up to 100−200 molecules in phase II occurs instantly (skipping phase I), depleting the dimeric protein in the solution below the detectable concentration limit. The third phase shifts the whole population of small polymers toward the larger polymers, i.e., the further growth up to 1000 or more molecules per polymer is established by the association or coalescence of correspondingly smaller polymers similar to a step-growth mechanism first treated by von Smoluchowski [55].

The striking difference between the two types of growth experiments induced by GTP or GDP*AlF$_x$ is further substantiated by the correlation of the radius of gyration R_g with the corresponding mass M_w of the growing particles (Fig. 5 D). The experiments where the polymerization is triggered by GTP instantaneously leads to a mixture of monomers and dimers, noticeable with a measurable size close to a radius of 20 nm (Fig. 5 B,D). Successively, the mass gradually increases by more than two orders of magnitudes with an increase of the radius by a factor of only 5. In contrast, in the experiments carried out in the presence of GDP*AlF$_x$ the drastic increase of the mass during the first 2 min at an R_g close to 25 nm shifts the onset of correlation to 10^7 g/mol (Fig. 5 D), well separated from the corresponding onset observed in the presence of GTP. Only after phase II is completed, does the third phase commence, which most likely progresses according to a step-growth process. Noticeably, the trends overlay for each type of experiments (Fig. 5 D), making this plot an efficient tool to discriminate between the mechanisms of the two types of nucleotides.

We hypothesize that phase II, leading to compact particles with R_g ~25 nm and M_w ~10^7 g/mol is the

one consuming the $hGBP1_{fn}$ dimers via the addition of dimer units. In the presence of GDP*AlF_x, this phase is too fast to be identified with a bimodal analysis of the field-time correlation function but fast enough to be unambiguously separated in time from phase III. This distinct separation of the two phases by 10 min in the presence of GDP*AlF_x also enabled us to observe the onset of an anisometry in shape from the beginning of phase III. In the presence of GTP, the two phases may just overlay throughout the entire time course of the experiments.

Taken together, we approved for GTP-dependent polymerization, that (1) the start is dominated by a dynamic equilibrium between monomers and bulky dimers and (2) that this monomer-dimer equilibration is followed by sequential addition of GTP-bound-monomer or -dimer in a chain reaction-like "monomer-addition process." With the help of the GTP transition state analog GDP*AlF_x, $hGBP1_{fn}$ directly forms small polymers without cycling in the monomer-dimer equilibrium. The same type of small polymer may also be formed in the presence of GTP, yet, without being identified as its generation is overlaid by its coalescence to larger polymers.

$hGBP1_{fn}$ loses its granular structure by interaction with nonfarnesylated hGBP1 within the cells

In cells, hGBP1 is located at the plasma membrane and appears as granular or vesicle-like structures in the cytosol [27]. This granular distribution is abolished when preventing farnesylation of hGBP1. Endogenous hGBP1 in cells treated with an FTase inhibitor, as well as an ectopically expressed hGBP1 mutant lacking the CaaX box, were found homogeneously distributed in the cytosol [27]. Here, we confirmed these findings by expressing the nonfarnesylated mutant hGBP1-C589S in HeLa cells, which lacks the CaaX box cysteine. Whereas wild type hGBP1 appeared as granular structures in the cytosol, the C589S mutant failed to do so (Fig. 6 A). Based on our previous study, where we demonstrated that hGBP1 is in a dynamic exchange with the cytosol and not stably membrane-associated [39], we hypothesized that a part of the observed granular structures represents hGBP1 polymers. We tested this hypothesis by co-expressing GFP-tagged hGBP1 wild type and mCherry-tagged hGBP1 mutants, which influenced polymerization in our biochemical experiments and tested localization and colocalization. In agreement with our turbidity assay, which showed that nonfarnesylated hGBP1 is not incorporated into the polymer and inhibits polymer formation, GFP-$hGBP1_{fn}$ and mCherry-hGBP1-C589S both displayed a homogenous distribution in the cytosol when co-expressed in HeLa cells (Fig. 6 B). Interestingly, GFP-hGBP1 and mCherry-hGBP1-R48A co-localized and appeared as granular structures, which were significantly larger than the structures observed for GFP- and mCherry-tagged wild type protein (Fig. 6 B). These larger structures formed by the R48A mutant and wild type protein were also confirmed with bimolecular fluorescence complementation (BiFC) analysis (SI Fig. S7). These observations support the notion that the granular structures might not only be identified as an accumulation of hGBPs around small vesicles, but rather as hGBP1 polymers.

Discussion

hGBP1 operates in cell-autonomous defense against numerous bacterial, viral, and protozoan pathogens [4,5,7,57]. These counteractions are mostly mediated by membrane binding, for which the farnesyl moiety is necessary. Next to membrane interaction, the farnesylation of the protein provides the ability of nucleotide-dependent, reversible polymerization. The biological significance of these polymers remains mostly unclear to the present stage. It is conceivable that the polymers serve as protein storages after interferon-induced, strong upregulation of hGBP1 synthesis. With this work, we want to gain a better understanding of the underlying mechanism of polymer formation.

In our previous work [39], negative stain electron microscopy revealed GTP dependent formation of disc-shaped polymers, and further growth by stacking of such entities was suggested. The different levels of GTPase activity were explained by different orientations of the LG domains within the polymers. We want to extend this model and to render it more precisely based on the observations described in this work. First, we could show that the mechanism of polymerization relies on different domain interactions between the $hGBP1_{fn}$ molecules successively established, directly after GTP-binding dimerization is induced by the interaction of the LG domains. These LG-contacts turned out to be crucial not only for dimer formation but also for the polymerization as confirmed by the experiments with the mutant R244A located in the LG:LG interface. Dimer formation precedes polymerization, and alternatively, it is also conceivable that polymer growth is performed by the addition of GTP-bound monomers, which attach to an LG domain at the periphery of the polymer.

What happens prior to polymer formation? Dimerization of $hGBP1_{fn}$, presumably as a dynamic equilibrium with the monomeric protein, dominates phase I. Within this lag phase of 3 min (for 10 μM hGBP1 at 25 °C) the protein undergoes 3–5 cycles of GTP hydrolysis, GDP release, and GTP rebinding. Of note, no GMP is formed at this early stage. Within this phase I, FRET reports that LG domains bind to each other immediately after the addition of GTP while donor and acceptor labels attached to the MD

do not respond initially. Only after the lag phase and most presumably concomitantly with the establishment of the first polymers (beginning of phase II) FRET increases reporting MD:MD proximity. One should make the point here that the reported MD:MD contacts do not necessarily go back to contacts within the dimer. In light of the delayed and slow kinetics, it is also conceivable that MDs approach each other only when built into the polymer. Along the same line, the opening of the structure, i.e., separation of the GED from the LG domain, should be considered. It is not immediately triggered by GTP binding, which is in contrast to the nonfarnesylated variant. Rather, the opening of $hGBP1_{fn}$ occurs simultaneously to the approach of the MDs to each other, and thereby simultaneously to the establishment of the first polymers. Thus, it is suggested that in the dimer, both GEDs swing open upon GTP hydrolysis, which presumably is supported by additional contacts between the C-terminal part, including the farnesyl moiety. The involvement of contacts between two α13 helices in dimerization was demonstrated by an earlier study on nonfarnesylated hGBP1 [36]. Once this stage is reached, this dimer is incorporated into the polymer leading to permanent stabilization of an outstretched structure, i.e., the GED having turned by 180°. The establishment of an opened and finally, outstretched dimer might represent the bottleneck for the initiation of polymerization. Multiple GTPase cycles are required to reach this – just as if it needs some attempts to present the outstretched dimer, which then readily associates with the polymer.

Intriguingly, in the first phase of polymerization low GTPase activity and no GMP production is observed. This can be rationalized by mechanical constraints due to intramolecular interactions within the enzyme that have to be overcome. Such constraints come up when GTP gets hydrolyzed, i.e., when changing from the GTP to the GDP bound state. For example, the intramolecular constraints reinforced by the farnesyl moiety may impede the structural change from the GTP to the GDP or GMP bound state. The tighter the interaction between LG and GED the lower the GTPase activity and the less GMP is produced: Starting with the covalently linked LG:GED variant with the tightest link between LG domain and GED, going on to wild type with a moderate affinity between LG and GED due to the salt bridges, and finally to the RK double mutant with the loss of these salt bridges, we previously observed an increasing GTPase activity and an increasing fraction of GMP produced [33,49]. In the first phase of polymerization, farnesylated hGBP1 fits seamless into this series as it shows only low GTPase activity and no GMP production, like the covalently linked LG:GED, since the farnesyl moiety contributes to the binding affinity between GED and the rest of the protein. Only after persistent opening, which is the case after incorporation into the polymer in phase II a high GTPase activity and a high level of GMP production are observed similar to the nonfarnesylated hGBP1. The importance of structural opening driven by GTPase activity for the mechanism of polymer formation is supported by the observations made with the RK double mutant. The loss of the LG:GED contact facilitates opening, which leads to immediate polymerization by skipping phase I.

Usually, the lag phase in a polymerization process is defined by the formation of the first polymer seeds acting as a nucleus for further growth. Our data suggest that nucleation is not the critical step for hGBP1 polymer formation as we do not see any lag phase for polymerization of the RK mutant and not for the polymerization of the wild type in the presence of GDP*AlF_x either. Both $hGBP1\text{-}RK_{fn}$ in the presence of GTP, and $hGBP1_{fn}$ in the presence of GDP*AlF_x exhibit a permanently open structure. There is no cycling between open and closed states like in the case of wild type and GTP, which produces fruitful open states for a short moment but may fall back to the unproductive closed state again and again. Therefore, we disfavor the idea of nucleation to be responsible for the lag phase but rather attribute the lag to the arduous opening of the structure driven by GTPase cycles, i.e., phase I.

Consistent with the previously published findings of Shydlovskyi et al. [39], that the farnesyl moiety is required for polymerization, our results reinforce this observation by showing that addition of polymerization partners without the farnesyl moiety (hGBP1) or without the helical parts of the protein (Δ-GED and LG) impair polymerization. On the one hand, these nonfarnesylated interaction partners hold $hGBP1_{fn}$ molecules back from incorporation in the polymer by the formation of a nonfruitful dimer harboring only one farnesyl moiety. On the other hand, the nonfarnesylated variant, when transiently incorporated into the polymer by coupling to a $hGBP1_{fn}$ molecule, destabilizes the polymer and makes it fall apart as each farnesyl moiety is critical for the fate of the whole polymer – bad spots cannot be tolerated. This view is further substantiated by our observations in HeLa cells. The cytosolic granular structures might represent the polymers since we could see in cells the same effect as *in vitro* when offering nonfarnesylated protein as a polymerization partner. *In vitro,* the disappearance of turbidity is seen upon the addition of nonfarnesylated hGBP1, while in the cells, the granular structures are dissolved, and the proteins distribute homogeneously in the cytosol when $hGBP1_{fn}$ is co-expressed with a nonfarnesylated variant. Furthermore, the importance of the farnesyl moiety for polymerization is supported by the observation that the addition of FPP shortens the lag phase. This extra FPP might lead to an enhanced

gluing effect of the hydrophobic center in the core of the polymer formed by the farnesyl moieties.

GTP hydrolysis activity is crucial for all aspects of $hGBP1_{fn}$ polymerization. It is responsible for the opening of the protein in phase I, which serves in its opened conformation as an entity building up the polymer. Not surprisingly, the polymer disassembles after all GTP is used up. Most likely, GDP, GMP, and P_i dissociate from $hGBP1_{fn}$, which is integrated into the polymer and GTP will rapidly rebind since a small fraction of $hGBP1_{fn}$ molecules without GTP could be stabilized in the opened structure by the neighboring molecules. Nevertheless, it is conceivable that single molecules leave the polymer after GTP hydrolysis,

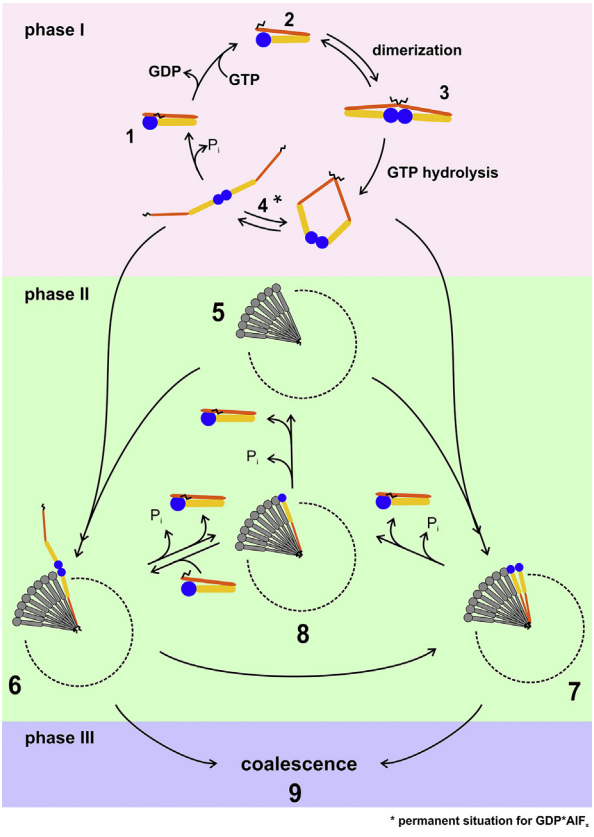

Fig. 7. Mechanism of $hGBP1_{fn}$ polymer formation. In phase I of polymerization (pink) $hGBP1_{fn}$ cycles between a closed (1) and more or less opened forms (2–4) in a nucleotide and enzymatic activity dependent manner. In phase II (green) the opened dimer (4) is incorporated in the polymer (5,6,7 gray). Upon GTP hydrolysis single $hGBP1_{fn}$ molecules may or may not dissociate from the polymer and may reassociate after passing through phase I again. Eventually, after depletion of GTP the polymer will dissolve completely. Coalescence of smaller polymers to yield larger ones (phase III) occurs in the presence of GTP, as well as GDP*AlF_x. Only in the case of the latter nucleotide this process is well separated on the time scale while in the presence of GTP there is overlap of dimer addition and coalescence mechanisms.

and it is also possible that single, GTP bound $hGBP1_{fn}$ molecules will add to the polymer as pointed out above. This part of the mechanism will become important when single $hGBP1_{fn}$ molecules have reached a low concentration and dynamic equilibrium with $hGBP1_{fn}$ molecules going on and off the polymer is established. We had previously reported that the GTPase deficient mutant R48A does not form polymers on its own. Here we show that it gets incorporated into the polymer in combination with the wild type. Again, we see two possible explanations. Preformed homodimers of hGBP1-$R48A_{fn}$ do not overcome the hurdle in phase I, which they can pass by forming a heterodimer with $hGBP1_{fn}$. Alternatively, a GTP-bound, monomeric hGBP1-$R48A_{fn}$ molecule forms a heterocomplex by attaching to a wild type LG domain at the periphery of the preformed polymer and then gets incorporated.

The scheme in Fig. 7 illustrates the mechanism of polymerization accounting for all details observed for $hGBP1_{fn}$ labeled by fluorophores at various positions, modified by mutations and bound to various nucleotides. The first phase of polymerization (pink) is dominated by a cycle between monomers and dimers. GTP binding evokes the release of the farnesyl moiety from the binding pocket, but it is not sufficient for opening the structure (2 in the scheme). This is based on the observations that the binding of nonhydrolyzable analogs like GTPγS and GppNHp trigger the attachment to lipid membranes through the farnesyl moiety but cannot initiate polymerization [39]. Nevertheless, these analogs are reported to lead to an equilibrium of monomer and dimer (3). It is also possible that the release of the farnesyl moiety occurs concomitantly with dimer formation. Further structural changes within $hGBP1_{fn}$ can only be achieved upon nucleotide hydrolysis, eventually leading to the opening of the structure (4). As pointed out, under constrained conditions, GTP hydrolysis is slow, and the hydrolysis of GDP as a second step does not happen. Rather, the dimer may fall apart, going back to the start (1). It may cycle like this a few times before the opened dimer is caught by the polymer (depicted in gray) (5), i.e., entering the cycle of polymer growth in phase II (green). The full opening of the dimer as transiently achieved through GTP hydrolysis is permanently established when $hGBP1_{fn}$ is bound to GDP*AlF_x (4). Thus, this species is not short-lived but can easily and without delay build the polymer as observed for $hGBP1_{fn}$-GDP*AlF_x, and the RK mutant in the presence of GTPγS. As substantiated above, the nucleation of $hGBP1_{fn}$ molecules is not the bottleneck for polymer formation. Growth of the polymer in phase II is conceived as the addition of an open dimer where one or two farnesyl moieties are heading for the hydrophobic center, and the protein is incorporated alongside the other molecules in the polymer (6 or 7) giving rise to MD:MD, as well as

LG:LG proximity, which was observed to develop coincidently with polymer growth. The second half of the dimer (6) may swing inwards to propagate growth (7). Alternatively, the LG domains may detach from each other as the GDP, or GMP state is established, and one half of the dimer may dissociate from the polymer (8) reentering as monomer the cycle of phase I. Once small polymers are formed facing LG domains outwards it could be possible for GTP bound $hGBP1_{fn}$ molecules to bind to such an LG domain as it happens when dimers are formed. In this way, the polymer grows through the addition of $hGBP1_{fn}$ monomers (going from 8 to 6), but still through the LG:LG contact and GTP hydrolysis mediated opening. After nucleotide hydrolysis leading to the GDP or the GMP bound state, the $hGBP1_{fn}$ molecule has the chance to release the products of hydrolysis and to rapidly rebind GTP, and thus, to stay in the polymer. Alternatively, the tendency to close the structure by LG:GED contact formation may win, and the $hGBP1_{fn}$ molecule will dissociate from the polymer (going from 7 to 8 and further to 5). When the GTP concentration decreases below some value or as soon as there is less GTP than GMP in the solution, the dissociation of $hGBP1_{fn}$ molecules will be the prevailing action, eventually leading to the dissolution of the polymer. Altogether the mechanism suggests a highly dynamic polymerization reaction allowing for growth, as well as shrinking of polymer entities. Finally, polymer particles may coalesce and contribute to polymer growth (9) as soon as polymers are generated in phase II large enough to do so. We term the process of coalescence phase III (violet), which in the presence of GDP*AlF_x is nicely separated from the dimer addition process in phase II (see Fig. 5 C). In the presence of GTP likely a shift from phase II to III, i.e., a shift from the dimer addition mechanism to coalescence will occur after some time when small polymer particles are formed, and less dimer is available in the solution.

For quite a number of proteins, the function is based on the formation of polymers. The most prominent examples may represent actin, tubulin, and dynamin. Like hGBP1, they have all in common that polymerization is controlled in some way by the bound nucleotide. Actin and tubulin build long filaments, which serve for directed movement or transport of cargo, and for example, the polymerization of dynamin leads to the deformation of lipid membranes. So far, the role of hGBP1 polymerization is not clear. Many interaction partners are reported like membranes and proteins from pathogens and like inflammasome proteins. hGBP1 comes in three variants, namely, evenly distributed in the cytoplasm, bound to plasma or endomembranes, and concentrated in granular or punctate structures inside the cell. In this context it is to be noted that hGBP1 is only synthesized to reach high intracellular concentration levels after interferon stimulation of the cell. Therefore, it is conceivable that this protein developed a mechanism that allows it to drop out partially from the intracellular environment and to form a kind of depot, which we described and analyzed here as polymerization. The reversible and highly dynamic formation of such a highly concentrated protein pool allows for the rapid retrieval of the protein whenever pathogen defense, covering of membranes, or other tasks demand this. Although the exact requirement of mobilized hGBP1 is still outstanding, we have elucidated here the molecular mechanism of the reversible and dynamic formation of an enzyme polymer, which is controlled by nucleotide binding and hydrolysis.

Methods and Materials

Protein synthesis and purification

The proteins were generated and purified according to our previously described procedures [37] and as described in the following paragraph. Nonfarnesylated hGBP1 was cloned into pQE80L expression vectors, expressed in *Escherichia coli* BL21(DE3)-CodonPlus RIL (Stratagene, Heidelberg, Germany). hGBP1 was farnesylated by incubating nonfarnesylated hGBP1 with farnesyl pyrophosphate (Cayman Chemicals, Ann Arbor, Michigan, USA) and FTase (ratio 1 : 2.5 : 0.02) in farnesylation buffer (50 mM Tris-HCl pH 7.9, 5 mM $MgCl_2$, 150 mM NaCl, 10 μM $ZnCl_2$) for 16 h at 4 °C in a glass vial. The reaction mixture was adjusted to a final concentration of 1.25 M $(NH_4)_2SO_4$ and applied to a Butyl Sepharose High-Performance Column (GE Healthcare, Munich, Germany) to separate farnesylated from nonfarnesylated protein (adapted from Refs. [38,39]). After loading of protein solution to a previously equilibrated column (high salt buffer: 50 mM Tris-HCl pH 7.9, 5 mM $MgCl_2$, 1.2 M $(NH_4)_2SO_4$), the concentration of ammonium sulfate was decreased to 0 M in four successive steps. Initially, the concentration of $(NH_4)_2SO_4$ was reduced to 60%, and then to 45% in a continuous gradient over 3 column volumes (CV) (elution of $hGBP1_{fn}$). In a third step, the concentration of $(NH_4)_2SO_4$ is further decreased continuously to 25% over 3.75 CV (elution of hGBP1), followed by a step to 0% $(NH_4)_2SO_4$. $hGBP1_{fn}$ was concentrated by ultrafiltration (Vivaspin 20; 10 kDa cut-off, Sartorius, Göttingen, Germany), and applied to a gel filtration chromatography column (Superdex 200 26/60, GE Healthcare, Munich, Germany) run with buffer C (50 mM Tris-HCl pH 7.9, 5 mM $MgCl_2$,

150 mM NaCl) to remove ammonium sulfate and isolate monomeric protein.

Bacterial synthesis and purification of truncated mutants of hGBP1 (hGBP1-LG (aa 1−327) and hGBP1-ΔGED (aa 1−418)) were performed as described for hGBP1 full length (for hGBP1-LG ultrafiltration was performed with Vivaspin 20; 5 kDa cut-off, Sartorius, Göttingen, Germany). hGBP1-Q577C_{fn} was expressed, purified, and farnesylated as described for hGBP1$_{fn}$, while the point mutants hGBP1-RK$_{fn}$, hGBP1-R244A$_{fn}$, and hGBP1-R48A$_{fn}$ were co-expressed with recombinant FTase and purified as described previously [38].

Labeling of protein with fluorescent dyes

Many of our experiments are based on FRET-based experiments. Therefore we produced two variants to study intermolecular processes like dimerization and polymerization, namely a variant, which is labeled predominantly at Cys396, termed MD labeled, and another variant labeled at Cys396 and additionally at Cys12 and/or Cys270, termed LG&MD labeled. This was defined by adjusting the temperature, concentration of the dye, and incubation time. The results were evaluated by SDS gel electrophoresis after limited tryptic digestion (see below). In order to track intramolecular processes, namely the opening of the enzyme, i.e., increasing the distance between GED and the LG domain/MD part, we produced a third variant labeled with two colors: the acceptor attached to the GED (Cys589 in the case of nonfarnesylated hGBP1 and Cys577 introduced by mutagenesis in the case of farnesylated hGBP1) and the donor attached to LG/MD. We used AlexaFluor488-C5-maleimide dye (Thermo Scientific, Waltham, MA, USA) as a donor and AlexaFluor647-C2-maleimide dye (Thermo Scientific, Waltham, MA, USA) as an acceptor in buffer L (50 mM Tris-HCl pH 7.4, 5 mM $MgCl_2$ 150 mM NaCl) on ice. In order to obtain the MD labeled hGBP1$_{fn}$, the protein was either incubated with acceptor fluorophore or with donor fluorophore (for 10 min and molar ratio: 1.0 each). For LG&MD labeled hGBP1$_{fn}$ the protein was incubated with either acceptor or donor fluorophore (both, molar ratio: 4.0 and 50 min). For two-color labeling of farnesylated proteins the mutation Q577C was generated by using a QuickChange site-directed mutagenesis kit according to the manufacturer's protocol (Merck, Darmstadt, Germany), for ensuring a labeling position at the C-terminus. The labeling procedure for two-color labeling (donor and acceptor dye on the same molecule) was established previously [37], and it is the same for all three constructs (hGBP1-Q577C$_{fn}$/hGBP1/hGBP1-RK-Q577C$_{fn}$ later referred to as hGBP1-RK$_{fn}$). The protein was labeled sequentially by incubating the protein with acceptor fluorophore using a molar ratio of 0.9 dye/protein for 10 min and directly afterward with the donor fluorophore using a molar ratio of 1.0 dye/protein for 5 min. All reactions were stopped by addition of 2 mM DTT. Unbound fluorophore was removed via buffer exchange (buffer C) followed by concentrating the protein by ultrafiltration (Vivaspin Turbo 4; 10 kDa cut-off, Sartorius, Göttingen, Germany). Labeling efficiencies were calculated from absorbance at wavelengths 280 nm (hGBP), 491 nm (Alexa488, donor) and 651 nm (Alexa647, acceptor) in buffer C + 2 mM DTT, using molar absorption coefficients of ϵ_{280}: 45,400 $(M*cm)^{-1}$, ϵ_{491}: 71,000 $(M*cm)^{-1}$, ϵ_{647}: 268,000 $(M*cm)^{-1}$, and the correction factors provided by the company. Labeling efficiencies were as follows: two-color-labeled: hGBP1$_{fn}$: LE_D: 58%, LE_A: 90%; hGBP1-RK$_{fn}$: LE_D: 54%, LE_A: 80%; hGBP1: LE_D: 86%, LE_A: 68%. MD-labeled hGBP1-$_{fn}$: LE_D: 31%, LE_A: 21%. LG&MD labeled hGBP1$_{fn}$: LE_D: 203%, LE_A: 90%.

In SI Fig. S2 we point out in more detail how we come to the assignment of the labeling positions. They are based on surface accessibility calculations [66], the observations after tryptic digestion, and on conclusions from FRET experiments. In SI Fig. S2 B, G we have also collated the relevant cysteine residue distances within the protein and within possible dimeric structures in order to compare them to the Förster radius.

Trypsin digestion

In order to define the domain of hGBP1 that is labeled, limited tryptic digestion was performed as described in Ref. [37]. In brief, labeled hGBP1 with a concentration of 1.15 g/l was digested with 0.005 g/l trypsin in buffer C at 25 °C. Samples were taken prior to trypsin addition and 1, 5, and 15 min after addition. The reaction was immediately stopped by the addition of SDS-sample buffer (125 mM Tris/HCl, pH 6.8, 50% glycerol, 10% SDS, 10 mM β-mercaptoethanol, and 0.01% bromophenol blue), followed by incubation at 95 °C for 5 min. Samples were analyzed by SDS-PAGE. The protein bands were fixed, and the fluorescence image was taken by exciting the fluorophores with a BioLite Multi-Spectral Source (UVP, Cambridge, UK) and detecting the fluorescence with a BioSpectrum Imaging System (UVP), using the respective excitation and emission filters. Afterward, protein bands were stained with Coomassie, and images were superimposed.

Intra- and intermolecular FRET

Intra- and intermolecular FRET measurements were performed on an LS55 fluorescence spectrometer (PerkinElmer, Waltham, MA, USA) in quartz glass cuvettes (Hellma Analytics, Mühlheim,

Germany) with a path length of 10 mm. The temperature was set to 25 °C if not indicated otherwise. The donor (Alexa488) was excited at 498 nm, and the acceptor (Alexa647) was detected at 664 nm. Excitation and emission slits were set to 10 and 15 nm, respectively and detector voltage was set to 775 mV. Measurements were carried out in buffer C or buffer C + AlF_x (buffer C + 10 mM NaF + 300 μM $AlCl_3$) with addition of 50 μM BSA. In total 2 μM of protein were incubated at 25 °C prior to nucleotide addition (1 mM GTP, 250 μM GTPγS, 250 μM GDP in order to form GDP*AlF_x, 1 mM GppNHp, 250 μM GMP, respectively). For intramolecular FRET 0.2 μM of two-color-labeled hGBP1-Q577C_{fn}/hGBP1/hGBP1-RK_{fn} was mixed with 1.8 μM of the corresponding nonlabeled protein ($hGBP1_{fn}$/hGBP1/hGBP1-RK_{fn}). To track intermolecular FRET between the middle domains donor and acceptor labeled $hGBP1_{fn}$ were mixed in equimolar concentrations. For LG-mediated intermolecular FRET 0.2 μM of donor-labeled $hGBP1_{fn}$ + 0.8 μM of acceptor-labeled $hGBP1_{fn}$ were mixed with 1 μM of nonlabeled $hGBP1_{fn}$. If not indicated otherwise, changes in fluorescence at 664 nm (F) were normalized by initial fluorescence (F_0) before nucleotide addition (fluorescence plotted as F/F_0). For the concentration-dependent intermolecular FRET measurements (Fig. S1 B and C, S3 C, S4 J), data were treated differently: For facilitating the comparability with the concentration-dependent absorbance measurements, the initial fluorescence prior to nucleotide addition was subtracted from the fluorescence time course (fluorescence plotted as F_{664}).

Rate constants of polymerization and of GTPase activity

Absorbance based measurements of polymerization were performed as described previously [39]. Briefly, different concentrations of protein were incubated in buffer C with 50 μM BSA at 25 °C for 5 min, and polymerization was induced by the addition of 1 mM GTP. Absorbance was measured at a wavelength of 350 nm, reflecting the loss of light intensity due to the scattering of the turbid solution. The scattering intensity I(scattered) depends on the wavelength λ of the transmitting light obeying a power law of I(scattered) ~ λ^{-4}. Hence, scattering and along with this, the absorption due to transmission losses drastically increases with decreasing wavelength. Therefore, a good measure of turbidity is the absorption/transmission of a liquid at a short wavelength, preferably not interfering with UV absorption of the protein. Nucleotide composition during polymerization was monitored by taking 2 μl-samples from the cuvette, stopping GTP hydrolysis by addition of 5 μl 10% H_3PO_4, and neutralization with 15 μl of 0.77 M K_2HPO_4. Nucleotide composition was further analyzed by separation of GTP, GDP, and GMP by reversed-phase HPLC (Chromolith Performance, RP-18 endcapped column (Merck, Darmstadt, Germany)). Elution of nucleotides was detected at 254 nm (MD-2010 Plus, Jasco, Pfungstadt, Germany), and peak areas were integrated and quantified with the manufactures software [58].

To reveal the polymer formation rate constant k_{ass}, the association process of the polymer, including the first phase and the growth phase up to reaching the maximal absorbance, can be modelled by eq. (1) also used to describe protein fibril formation [59,60].

$$y = y_i + m_i{*}x + \frac{y_f + m_f{*}x}{1 + e^{\frac{-(x-x_0)}{\tau}}} \quad (1)$$

The half-maximal signal is reached after time x_0, and the apparent elongation rate constant of the polymer is $k_{app} = \tau^{-1}$. k_{app} shows a linear dependence on the protein concentration, where k_{ass} equals the slope.

Dynamic light scattering

A dynamic light scattering of nonfarnesylated and farnesylated hGBP1 and hGBP1-RK was performed on a HPPS-High Performance Particle Sizer (Malvern Instruments, Malvern, UK). 10 μM of protein were incubated at 25 °C in a total sample volume of 400 μl in buffer C or buffer C + AlF_x. Measurements were started directly after nucleotide addition (250 μM GDP or GTPγS, 1 mM GppNHp). The change in the particle size was measured in two independent measurements over 8–10 data points, and the mean diameter of the particles were determined by the manufacture's software. The results of this type of experiments are displayed in SI Fig. S3 C.

Combined static and dynamic light scattering

Time-resolved static (SLS) and dynamic light scattering (DLS) measurements were performed on an ALV/CGS-3/MD-8 multidetection system (ALV Laservertriebsgesellschaft, Langen, Germany). A He–Ne laser was used as a light source, with a wavelength of $\lambda_0 = 632.8$ nm and a power of 35 mW. The instrument consists of an array of eight detectors with two neighboring detectors separated by 8°, covering an angular range of $30° \leq \theta \leq 86°$, which corresponds to a q-range in water of $6.3.10^{-3} \leq q \leq 18.10^{-3}$ nm^{-1} with

$$q = \frac{4\pi n}{\lambda_0} \cdot \sin\left(\frac{\theta}{2}\right) \quad (2)$$

being the momentum transfer, $n = 1.332$ (at $T = 25$ °C), the refractive index of water, θ the scattering angle, and λ_0 the laser wavelength in vacuum. The time resolution of time-resolved SLS/

DLS experiments was 10 s, corresponding to the time needed to acquire an angular dependent set of SLS/DLS data.

The excess Rayleigh ratio ΔR of the solute is provided by SLS

$$\Delta R = RR_{\theta,std}\frac{\left(r_{\theta,sol} - r_{\theta,solv}\right)}{r_{\theta,std}} \tag{3}$$

With $RR_{\theta,std}$ the absolute Rayleigh ratio of toluene as standard and with $r_{\theta,sol}$, $r_{\theta,solv}$ and $r_{\theta,std}$ the measured scattering signal of the solution, the solvent, and toluene, respectively. Data were treated with the Guinier approximation [61]

$$\ln\left(\frac{Kc}{\Delta R}\right) = \ln\left(\frac{1}{M_w e^{\left(-\frac{R_g^2 q^2}{3} + B\cdot q^4\right)}}\right) \tag{4}$$

where the factor $B\cdot q^4$ is introduced to take into account a bending of the scattering curves. In eq. (4), c is the mass concentration of protein and K is the contrast factor

$$K = \frac{4\pi^2 n^2}{N_A \lambda^4}\left(\frac{dn}{dc}\right)^2 \tag{5}$$

with Avogadro's number N_A and the refractive index increment dn/dc of hGBP1 in buffered solution. A value of $dn/dc = 0.185$ ml/g was used for hGBP1, as being typical for proteins [62]. Obtained values for M_w and R_g have to be considered as apparent because time-resolved measurements could not be extrapolated to the infinite dilution limit. However, the investigated concentrations usually justify the neglecting of interparticle interactions.

DLS provides the field correlation function $g_1(\tau)$, which was treated in two different ways to gain information about the hydrodynamic properties of the investigated samples. A cumulant analysis was applied [63].

$$\ln(g_1(\tau)) = C - \Gamma(q)\cdot\tau + \frac{\mu_2}{2\Gamma^2}\tau^2 \tag{6}$$

with C a constant and $\Gamma(q)$ the mean inverse relaxation time of diffusive modes, which is given by the initial slope of $\ln(g_1(\tau))$.

An alternative method of data evaluation was used in the case of field correlation functions with two distinguishable decays, indicating two species in solution, which differ in size. In such a case, field correlation functions were evaluated with a biexponential approach.

$$g_1(\tau, q) = a(q) + b_1(q)\cdot exp(-\tau\cdot\Gamma_1(q)) + b_2\cdot exp(-\tau\cdot\Gamma_2(q)) \tag{7}$$

In eq. (8) $a(q)$ is the incoherent background, $b_i(q)$ is the intensity weighted weighing factor, and $\Gamma_i(q)$ is the inverse relaxation time of species i at angle q, *respectively*.

The z-averaged diffusion coefficient D_0 is obtained as the intercept of $\Gamma(q)/q^2$ vs q^2 at $q = 0$.

$$D_z = \frac{\Gamma(q)}{q^2} = D_0 + C_D \cdot R_g^2 \cdot q^2 \tag{8}$$

$D_z(q)$ is the apparent diffusion coefficient at angle q, and C_D is a shape sensitive constant. No concentration dependence of D_0 was considered for the same reason as mentioned in the context of SLS data.

The hydrodynamically effective radius R_h is calculated with the Stokes-Einstein relationship

$$R_h = \frac{k_b T}{6\pi\eta D_0} \tag{9}$$

Where k_b is the Boltzmann constant, T is the temperature in Kelvin, and η is the dynamic viscosity of the solvent (0.897 mPa*s (25 °C), 1.1 mPa*s (15 °C).

The size parameters R_g and R_h are used to calculate the structure sensitive parameter ρ.

$$\rho = \frac{R_g}{R_h} \tag{10}$$

The ratio ρ adopts values characteristic for the respective particle shape. Typical values are $\rho = 0.77$ for compact spheres, $1.2 < \rho < 1.6$ for polymer coils and $\rho > 2$ for rod-like particles [53,64]. The results obtained employing these techniques are displayed in Fig. 5 and in SI Fig. S4.

Sample preparation for static and dynamic light scattering experiments

A solution of 15 μM $hGBP1_{fn}$ was freshly prepared either in buffer C or in buffer C + AlF_x to reach a sample volume of 2.5 ml. The samples were then filtered (0.45 μm, PES-membrane, Acrodisc Supor) into cylindrical quartz cuvettes with a diameter of 24 mm (Hellma Analytics, Mühlheim, Germany), whereby the first 0.5 ml were used to equilibrate the filter and discarded. Time-dependent SLS/DLS measurements were then carried out at 25 °C with buffer C + AlF_x or at 15 °C with buffer C. Ten SLS/DLS measurements were carried out prior to the

addition of the initiating solution (GDP or GTP) in order to characterize the initial state of the solution. Successively, 1.5 ml of a freshly prepared solution containing either 3 mM GTP (for buffer C) or 750 μM of GDP (for buffer C + AlF_x) in buffer C was filtered (0.45 μm, PES-membrane, Acrodisc Supor) into the cuvette in order to initiate the polymerization, whereby the first 0.5 ml were used to equilibrate the filter and discarded. Thus, the sample volume inside the cuvette then amounts to 3 ml, leading to final concentrations of 10 μM for $hGBP1_{fn}$, 1 mM for GTP, and 250 μM for GDP*AlF_x. After gently shaking the cuvette to ensure homogeneity, time-resolved SLS/DLS measurements were carried out with time zero corresponding to the addition of the nucleotide. Experiments were by default carried out without BSA since it has a similar size as hGBP1, and thus, would interfere with the signal on the monomeric state of hGP1 or on the state of small oligomers. Nevertheless, in order to ensure comparability with the other experiments of this work, the SLS/DLS measurements were carried out, as well as with buffers, including 50 μM BSA.

Cell culture

Plasmids

The plasmids pMCV1.4 (−) and (+) were obtained from Mologen (Berlin, Germany). A Flag−tag sequence (abbreviation: F) was cloned into the pMCV1.4(−) plasmids using *Eco*RV/*Eco*RI restriction sites, followed by the in-frame insertion of the GFP sequence into pMCV1.4-Flag using the *Eco*RI restriction site. For obtaining a GFP-GBP1 fusion protein the GBP1 sequence (NCBI accession number: NM_002053.2) was inserted into the pMCV1.4-Flag-GFP vector using *Sna*BI and *Sal*I restriction sites. To obtained mCherry fusion proteins, the sequence of hGBP1 or hGBP1-C589S was cut out of the pQE80L vector using *Bam*HI and *Sal*I restriction enzymes, and cloned into the pmCherry-C1 vector using the *Bgl*II and *Sma*I restriction sites. The mutant mCherry-hGBP1-R48A was obtained by site-directed mutagenesis of pmCherry-C1-hGBP1 using the QuickChange site-directed mutagenesis kit according to the manufacturer's protocol (Merck, Darmstadt, Germany). For bimolecular fluorescence complementation (BiFC) analysis, plasmids were cloned as previously described [27]. Briefly, the coding sequences of GBP1 and GBP1-R48A were inserted into pMCV1.4-Venus1 and pMCV1.4-VSV-Venus2, respectively, in 3′ of the Venus sequence using *Eco*RV and *Xho*I restriction sites.

Cell culture and transfections

HeLa cells were purchased from ATCC and cultured in DMEM supplemented with 10% (v/v) fetal bovine serum (FBS) from Gibco (Thermo Fisher Scientific, Dreieich, Germany). One day prior transfection, HeLa cells were seeded in Lab-Tek chamber slides (Nunc™, Thermo Fisher Scientific). One microgram of plasmid was transfected per well using the calcium phosphate method [65].

Fluorescence microscopy

Twenty-four hours after transfection, cells were fixed in 10% buffered formalin and permeabilized with 0.1% Triton X100 (both from Sigma-Aldrich). Nuclei were counterstained with Draq5 (1:800 in water, Cell Signaling Technology, Frankfurt am Main, Germany) for 10 min at room temperature. Coverslips were mounted in fluorescence mounting medium (Dako, Hamburg, Germany). Fluorescence was visualized using the confocal microscope, TCS SPE (Leica Microsystems, Wetzlar, Germany) using a 63x magnification. Pictures were obtained using the LAS AF software (Leica Microsystems). The following excitation wavelengths (Ex) and spectral detection windows of the photomultiplier (PM) were used: for GFP, Ex = 488 nm, PM: 500−625 nm; for Venus-1/Venus-2, Ex = 488 nm, PM: 492−610 nm; for mCherry, Ex = 561 nm, PM = 565−674 nm and for Draq5, Ex = 635 nm, PM = 650−750 nm. Laser power was 10 mW (488 nm), 10 mW (561 nm) and 18 mW (635 nm), and intensity was set between 50 and 60% for all three lasers. All images presented are single sections in the z-plane (airy unit = 1) and are representative of at least 80% of the transfected cells.

Acknowledgement

Supporting grants were from the German Research Foundation (DFG) FOR 2438 [subproject 2 to MS], SFB/TRR241 [subproject A06 to MS and NBL], and HE2679/6−1 to CH.

Author Contributions

Linda Sistemich: Investigation, Visualization, Writing - Original Draft **Miriam Kutsch:** Investigation, Writing - Review & Editing **Benjamin Hämisch:** Investigation, Visualization **Ping Zhang:** Investigation **Sergii Shydlovskyi:** Investigation **Nathalie Britzen-Laurent:** Investigation, Visualization **Michael Stürzl:** Methodology, Writing − Review & Editing **Klaus Huber:** Methodology, Writing - Review & Editing **Christian Herrmann:** Conceptualization, Methodology, Writing − Original Draft, Review& Editing.

Appendix A. Supplementary data

Supplementary data to this article can be found online at https://doi.org/10.1016/j.jmb.2020.02.009.

Received 11 December 2019;
Received in revised form 30 January 2020;
Accepted 9 February 2020
Available online 19 February 2020

Keywords:
large GTPase;
GBPs;
dimer;
lag phase;
polymerization

Abbreviations used:
hGBP, human guanylate-binding protein; GTPyS, guanosine 5′-O-[γ-thio]triphosphate; GppNHp, guanosine 5'-[(β,γ)-imido]triphosphate; GDP*AlFx, guanosine diphosphate aluminum fluoride; MD, middle domain; GED, GTPase effector domain; LG-domain, large GTPase domain; FRET, Förster resonance energy transfer; FPP, farnesyl pyrophosphate; DSP, dynamin superfamily proteins.

References

[1] D. Danino, J.E. Hinshaw, Dynamin family of mechanoenzymes, Curr. Opin. Cell Biol. 13 (2001) 454–460, https://doi.org/10.1016/S0955-0674(00)00236-2.
[2] G.J.K. Praefcke, H.T. McMahon, The dynamin superfamily: universal membrane tubulation and fission molecules? Nat. Rev. Mol. Cell Biol. 5 (2004) 133–147, https://doi.org/10.1038/nrm1313.
[3] J.D. MacMicking, Interferon-inducible effector mechanisms in cell-autonomous immunity, Nat. Rev. Immunol. 12 (2012) 367–382, https://doi.org/10.1038/nri3210.
[4] D. Pilla-Moffett, M.F. Barber, G.A. Taylor, J. Coers, Interferon-Inducible GTPases in host resistance, inflammation and disease, J. Mol. Biol. 428 (2016) 3495–3513, https://doi.org/10.1016/J.JMB.2016.04.032.
[5] G.J.K. Praefcke, Regulation of innate immune functions by guanylate-binding proteins, Int. J. Med. Microbiol. 308 (2017) 237–245, https://doi.org/10.1016/j.ijmm.2017.10.013.
[6] J.C. Santos, P. Broz, Sensing of invading pathogens by GBPs : at the crossroads between cell-autonomous and innate immunity, J. Leukoc. Biol. 104 (2018) 729–735, https://doi.org/10.1002/JLB.4MR0118-038R.
[7] S. Ming, M. Rajendra, K.T. Kanneganti, Molecular mechanisms and functions of pyroptosis, inflammatory caspases and inflammasomes in infectious diseases, Immunol. Rev. 277 (2017) 61–75, https://doi.org/10.1111/imr.12534.
[8] E. Braun, D. Hotter, L. Koepke, F. Zech, R. Groß, K.M.J. Sparrer, J.A. Müller, C.K. Pfaller, E. Heusinger, R. Wombacher, K. Sutter, U. Dittmer, M. Winkler, G. Simmons, M.R. Jakobsen, K.-K. Conzelmann, S. Pöhlmann, J. Münch, O.T. Fackler, F. Kirchhoff, D. Sauter, Guanylate-binding proteins 2 and 5 exert broad antiviral activity by inhibiting furin-mediated processing of viral envelope proteins, Cell Rep. 27 (2019) 2092–2104, https://doi.org/10.1016/j.celrep.2019.04.063.
[9] N. Britzen-Laurent, C. Herrmann, E. Naschberger, R.S. Croner, M. Stürzl, Pathophysiological role of guanylate-binding proteins in gastrointestinal diseases, World J. Gastroenterol. 22 (2016) 6434–6443, https://doi.org/10.3748/wjg.v22.i28.6434.
[10] F. Fellenberg, T.B. Hartmann, R. Dummer, D. Usener, D. Schadendorf, GBP-5 splicing Variants : new guanylate-binding proteins with tumor-associated expression and antigenicity, J. Invest. Dermatol. 122 (2004) 1510–1517, https://doi.org/10.1111/j.0022-202X.2004.22613.x.
[11] E. Guenzi, K. Töpolt, E. Cornali, C. Lubeseder-Martellato, A. Jörg, K. Matzen, C. Zietz, E. Kremmer, F. Nappi, M. Schwemmle, C. Hohenadl, G. Barillari, E. Tschachler, P. Monini, B. Ensoli, M. Stürzl, The helical domain of GBP-1 mediates the inhibition of endothelial cell proliferation by inflammatory cytokines, EMBO J. 20 (2001) 5568–5577, https://doi.org/10.1093/emboj/20.20.5568.
[12] W.H. Witola, E. Mui, A. Hargrave, S. Liu, M. Hypolite, A. Montpetit, P. Cavailles, C. Bisanz, M.-F. Cesbron-Delauw, G.J. Fournie, R. McLeod, NALP1 influences susceptibility to human congenital toxoplasmosis , proinflammatory cytokine response , and fate of Toxoplasma gondii -infected monocytic cells, Infect. Immun. 79 (2011) 756–766, https://doi.org/10.1128/IAI.00898-10.
[13] L. Gov, C.A. Schneider, T.S. Lima, W. Pandori, M.B. Lodoen, NLRP3 and potassium efflux drive rapid IL-1 β release from primary human monocytes during Toxoplasma gondii infection, J. Immunol. 199 (2017) 2855–2864, https://doi.org/10.4049/jimmunol.1700245.
[14] D. Fisch, H. Bando, B. Clough, V. Hornung, M. Yamamoto, A.R. Shenoy, E. Frickel, Human GBP 1 is a microbe-specific gatekeeper of macrophage apoptosis and pyroptosis, EMBO J. 38 (2019), https://doi.org/10.15252/embj.2018100926.
[15] L. Gov, Al Karimzadeh, N. Ueno, M.B. Lodoen, Human innate immunity to Toxoplasma gondii is mediated by host caspase-1 and ASC and parasite GRA15, mBio 4 (2013), https://doi.org/10.1128/mBio.00255-13 e00255-13.
[16] W. Niedelman, J.K. Sprokholt, B. Clough, E. Frickel, J.P.J. Saeij, Cell death of gamma interferon-stimulated human fibroblasts upon Toxoplasma gondii infection induces early parasite egress and limits, Infect. Immun. 81 (2013) 4341–4349, https://doi.org/10.1128/IAI.00416-13.
[17] A.S. Piro, D. Hernandez, S. Luoma, E.M. Feeley, R. Finethy, A. Yirga, E.M. Frickel, C.F. Lesser, J. Coers, Detection of cytosolic Shigella flexneri via a C-terminal triple-arginine motif of GBP1 inhibits actin-based motility, mBio 8 (2017), https://doi.org/10.1128/mBio.01979-17 e01979-17.
[18] P. Li, W. Jiang, Q. Yu, W. Liu, P. Zhou, J. Li, J. Xu, B. Xu, F. Wang, F. Shao, Ubiquitination and degradation of GBPs by a Shigella effector to suppress host defence, Nature 551 (2017) 373–383, https://doi.org/10.1038/nature24467.
[19] C. Krapp, D. Hotter, A. Gawanbacht, P.J. McLaren, S.F. Kluge, C.M. Stürzel, K. Mack, E. Reith, S. Engelhart,

A. Ciuffi, V. Hornung, D. Sauter, A. Telenti, F. Kirchhoff, Guanylate binding protein (GBP) 5 is an interferon-inducible inhibitor of HIV-1 infectivity, Cell Host Microbe 19 (2016) 504–514, https://doi.org/10.1016/j.chom.2016.02.019.

[20] R. Finethy, S. Luoma, N. Orench-Rivera, E.M. Feeley, A.K. Haldar, M. Yamamoto, T.-D. Kanneganti, M.J. Kuehn, J. Coers, Inflammasome activation by bacterial outer membrane vesicles requires guanylate binding proteins, mBio 8 (2017), https://doi.org/10.1128/mBio.01188-17 e01188-17.

[21] V. Lindenberg, K. Mölleken, E. Kravets, S. Stallmann, J.H. Hegemann, D. Degrandi, K. Pfeffer, Broad recruitment of mGBP family members to Chlamydia trachomatis inclusions, PloS One 12 (2017), e0185273, https://doi.org/10.1371/journal.pone.0185273.

[22] J. Coers, Sweet host revenge: galectins and GBPs join forces at broken membranes, Cell Microbiol. 19 (2018), https://doi.org/10.1111/cmi.12793.Sweet.

[23] E. Kravets, D. Degrandi, S. Weidtkamp-Peters, B. Ries, C. Konermann, S. Felekyan, J.M. Dargazanli, G.J.K. Praefcke, C.A.M. Seidel, L. Schmitt, S.H.J. Smits, K. Pfeffer, The GTPase activity of murine guanylate-binding protein 2 (mGBP2) controls the intracellular localization and recruitment to the parasitophorous vacuole of Toxoplasma gondii, J. Biol. Chem. 287 (2012) 27452–27466, https://doi.org/10.1074/jbc.M112.379636.

[24] E. Kravets, D. Degrandi, Q. Ma, T. Peulen, V. Klümpers, S. Felekyan, R. Kuehnemuth, S. Weidtkamp-Peters, C.A.M. Seidel, K. Pfeffer, Guanylate binding proteins directly attack Toxoplasma gondii via supramolecular complexes, Elife 5 (2016) e11479, https://doi.org/10.7554/eLife.11479.

[25] J.T. Stickney, J.E. Buss, Murine guanylate-binding protein: incomplete geranylgeranyl isoprenoid modification of an Interferon −γ− inducible guanosine triphosphate- binding protein, Mol. Biol. Cell 11 (2000) 2191–2200, https://doi.org/10.1091/mbc.11.7.2191.

[26] D.E. Nantais, M. Schwemmle, J.T. Stickney, D.J. Vestal, J.E. Buss, Prenylation of an interferon-γ-induced GTP-binding protein: the human guanylate binding protein, huGBP1, J. Leukoc. Biol. 60 (1996) 423–431, https://doi.org/10.1002/jlb.60.3.423.

[27] N. Britzen-Laurent, M. Bauer, V. Berton, N. Fischer, A. Syguda, S. Reipschläger, E. Naschberger, C. Herrmann, M. Stürzl, Intracellular trafficking of guanylate-binding proteins is regulated by heterodimerization in a hierarchical manner, PloS One 5 (2010), e14246, https://doi.org/10.1371/journal.pone.0014246.

[28] P.S.M. Schwemmle, The interferon-induced 67-kDa guanylate-binding protein (hGBP1) is a GTPase that converts GTP to GMP, J. Biol. Chem. 268 (1994) 11299–11305.

[29] A. Ghosh, G.J.K. Praefcke, L. Renault, A. Wittinghofer, C. Herrmann, How guanylate-binding proteins achieve assembly-stimulated processive cleavage of GTP to GMP, Nature 440 (2006) 101–104, https://doi.org/10.1038/nature04510.

[30] S. Kunzelmann, G.J.K. Praefcke, C. Herrmann, Transient kinetic investigation of GTP hydrolysis catalyzed by interferon-y-induced hGBP1 (human guanylate binding protein 1), J. Biol. Chem. 281 (2006) 28627–28635, https://doi.org/10.1074/jbc.M604911200.

[31] B. Prakash, G.J.K. Praefcke, L. Renault, A. Wittinghofer, C. Herrmann, Structure of human guanylate-binding protein 1 representing a unique class of GTP-binding proteins, Nature 403 (2000) 567–571, https://doi.org/10.1038/35000617.

[32] B. Prakash, L. Renault, G.J.K. Praefcke, C. Herrmann, A. Wittinghofer, Triphosphate structure of guanylate-binding protein 1 and implications for nucleotide binding and GTPase mechanism, EMBO J. 19 (2000) 4555–4564, https://doi.org/10.1093/emboj/19.17.4555.

[33] T. Vöpel, A. Syguda, N. Britzen-Laurent, S. Kunzelmann, M.B. Lüdemann, C. Dovengerds, M. Stürzl, C. Herrmann, Mechanism of GTPase-activity-induced self-assembly of human guanylate binding protein 1, J. Mol. Biol. 400 (2010) 63–70, https://doi.org/10.1016/j.jmb.2010.04.053.

[34] G.J.K. Praefcke, M. Geyer, M. Schwemmle, H.R. Kalbitzer, C. Herrmann, Nucleotide-binding characteristics of human guanylate-binding protein 1 (hGBP1) and identification of the third GTP-binding motif, J. Mol. Biol. 292 (1999) 321–332, https://doi.org/10.1006/jmbi.1999.3062.

[35] A. Syguda, A. Kerstan, T. Ladnorg, F. Stu, C. Wo, C. Herrmann, Immobilization of biotinylated hGBP1 in a defined orientation on surfaces is crucial for uniform interaction with analyte proteins and catalytic activity, Langmuir 28 (2012) 6411–6418, https://doi.org/10.1021/la3008359.

[36] T. Voepel, C.S. Hengstenberg, T. Peulen, Y. Ajaj, C.A.M. Seidel, C. Herrmann, J.P. Klare, Triphosphate induced dimerization of human guanylate binding protein 1 involves association of the C - terminal helices: a joint double electron – electron resonance and FRET study, Biochemistry 53 (2014) 4590–4600, https://doi.org/10.1021/bi500524u.

[37] S. Ince, M. Kutsch, S. Shydlovskyi, C. Herrmann, The human guanylate-binding proteins hGBP-1 and hGBP-5 cycle between monomers and dimers only, FEBS J. 284 (2017) 2284–2301, https://doi.org/10.1111/febs.14126.

[38] J.M. Fres, S. Müller, G.J.K. Praefcke, Purification of the CaaX-modified, dynamin-related large GTPase hGBP1 by coexpression with farnesyltransferase, J. Lipid Res. 51 (2010) 2454–2459, https://doi.org/10.1194/jlr.D005397.

[39] S. Shydlovskyi, A.Y. Zienert, S. Ince, C. Dovengerds, A. Hohendahl, J.M. Dargazanli, A. Blum, S.D. Günther, N. Kladt, M. Stürzl, A.C. Schauss, M. Kutsch, A. Roux, G.J.K. Praefcke, C. Herrmann, Nucleotide-dependent farnesyl switch orchestrates polymerization and membrane binding of human guanylate-binding protein 1, Proc. Natl. Acad. Sci. Unit. States Am. 114 (2017) E5559–E5568, https://doi.org/10.1073/pnas.1620959114.

[40] C. Ji, S. Du, P. Li, Q. Zhu, X. Yang, C. Long, J. Yu, F. Shao, J. Xiao, Structural mechanism for guanylate-binding proteins (GBPs) targeting by the Shigella E3 ligase IpaH9.8, PLoS Pathog. 16 (2019), e1007876.

[41] J.R. Jimah, J.E. Hinshaw, Structural insights into the mechanism of dynamin superfamily proteins, Trends Cell Biol. 29 (2018) 257–273, https://doi.org/10.1016/j.tcb.2018.11.003.

[42] M.G.J. Ford, J.S. Chappie, The structural biology of the dynamin-related proteins: new insights into a diverse, multitalented family, Traffic 20 (2019) 717–740, https://doi.org/10.1111/tra.12676.

[43] D.J. Vestal, V.Y. Gorbacheva, G.C. Sen, Different subcellular localizations for the related interferon-induced GTPases, MuGBP-1 and MuGBP-2: implications for different functions? J. Interferon Cytokine Res. 20 (2000) 991–1000, https://doi.org/10.1089/10799900050198435.

[44] P.J. Macdonald, N. Stepanyants, N. Mehrotra, J.A. Mears, X. Qi, H. Sesaki, R. Ramachandran, A dimeric equilibrium intermediate nucleates Drp1 reassembly on mitochondrial membranes for fission, MBoC 25 (2014) 1905–1915, https://doi.org/10.1091/mbc.E14-02-0728.

[45] S. Gao, A. Von der Malsburg, A. Dick, K. Faelber, G.F. Schröder, O. Haller, G. Kochs, O. Daumke, Structure of myxovirus resistance protein A reveals intra- and intermolecular domain interactions required for the antiviral function, Immunity 35 (2011) 514–525, https://doi.org/10.1016/j.immuni.2011.07.012.

[46] C. Patzina, O. Haller, G. Kochs, Structural requirements for the antiviral activity of the human MxA protein against Thogoto and influenza A virus, J. Biol. Chem. 289 (2014) 6020–6027, https://doi.org/10.1074/jbc.M113.543892.

[47] A.R. Shenoy, D.A. Wellington, P. Kumar, H. Kassa, C.J. Booth, P. Cresswell, J.D. MacMicking, GBP5 promotes NLRP3 inflammasome assembly and immunity in mammals, Science (80-.) 336 (2012) 481–485, https://doi.org/10.1126/science.1217141.

[48] R. Finethy, I. Jorgensen, A.K. Haldar, M.R. De Zoete, T. Strowig, R.A. Flavell, M. Yamamoto, U.M. Nagarajan, E.A. Miao, J. Coers, Guanylate binding proteins enable rapid activation of canonical and noncanonical inflammasomes in Chlamydia -infected macrophages, Infect. Immun. 83 (2015) 4740–4749, https://doi.org/10.1128/IAI.00856-15.

[49] T. Vöpel, S. Kunzelmann, C. Herrmann, Nucleotide dependent cysteine reactivity of hGBP1 uncovers a domain movement during GTP hydrolysis, FEBS Lett. 583 (2009) 1923–1927, https://doi.org/10.1016/j.febslet.2009.05.027.

[50] M. Kutsch, S. Ince, C. Herrmann, Homo and hetero dimerisation of the human guanylate- binding proteins hGBP-1 and hGBP-5 characterised by affinities and kinetics, FEBS J. 285 (2019), https://doi.org/10.1111/febs.14459, 2019–2036.

[51] M. Wehner, S. Kunzelmann, C. Herrmann, The guanine cap of human guanylate-binding protein 1 is responsible for dimerization and self-activation of GTP hydrolysis, FEBS J. 279 (2012) 203–210, https://doi.org/10.1111/j.1742-4658.2011.08415.x.

[52] G.J.K. Praefcke, S. Kloep, U. Benscheid, H. Lilie, B. Prakash, C. Herrmann, Identification of residues in the human guanylate-binding protein 1 critical for nucleotide binding and cooperative GTP hydrolysis, J. Mol. Biol. 344 (2004) 257–269, https://doi.org/10.1016/j.jmb.2004.09.026.

[53] W. Burchard, Static and dynamic light scattering from branched polymers and biopolymers, in: Light Scatt. From Polym., Springer Berlin Heidelberg, Berlin, Heidelberg, 1983, pp. 1–124.

[54] M.L. Mansfield, J.F. Douglas, S. Irfan, E. Kang, Comparison of approximate methods for calculating the friction coefficient and intrinsic viscosity of nanoparticles and macromolecules, Macromolecules 40 (2007) 2575–2589, https://doi.org/10.1021/ma061069f.

[55] M.v. Smoluchowski, Versuch einer Mathematischen Theorie der Koagulationskinetik Kolloider Lösungen, Z. Phys. Chem. 92 (1918) 129–168, https://doi.org/10.1515/zpch-1918-9209.

[57] E. Meunier, P. Broz, Microreview Interferon-inducible GTPases in cell autonomous and innate immunity, Cell Microbiol. 18 (2016) 168–180, https://doi.org/10.1111/cmi.12546.

[58] S. Kunzelmann, G.J.K. Praefcke, C. Herrmann, Nucleotide binding and self-stimulated GTPase activity of human guanylate-binding protein 1 (hGBP1), Methods Enzymol. 404 (2005) 512–527, https://doi.org/10.1016/S0076-6879(05)04045-0.

[59] M. Kutsch, P. Hortmann, C. Herrmann, S. Weibels, H. Weingärtner, Dissecting ion-specific from electrostatic salt effects on amyloid fibrillation: a case study of insulin, Biointerphases 11 (2016), 019008, https://doi.org/10.1116/1.4941008.

[60] L. Nielsen, R. Khurana, A. Coats, S. Frokjaer, J. Brange, S. Vyas, V.N. Uversky, A.L. Fink, Effect of environmental factors on the kinetics of insulin fibril formation, Biochemistry 40 (2001) 6036–6046, https://doi.org/10.1021/Bi002555c.

[61] A. Guinier, G. Fournet, Small-Angle Scatterubg of X-Rays, John Wiley & Sons, Inc., 1955.

[62] H. Zhao, P.H. Brown, P. Schuck, On the distribution of protein refractive index increments, Biophys. J. 100 (2011) 2309–2317, https://doi.org/10.1016/j.bpj.2011.03.004.

[63] D.E. Koppel, Analysis of macromolecular polydispersity in intensity correlation Spectroscopy : the method of cumulants, J. Chem. Phys. 57 (1972) 4814–4820.

[64] M. Schmidt, Combined integrated and dynamic light scattering by poly(7-benzyl glutamate) in a heliogenic solvent, Macromolecules 17 (1984) 553–560, https://doi.org/10.1021/ma00134a008.

[65] C.A. Chen, H. Okayama, Calcium phosphate-mediated gene transfer: a highly efficient transfection system for stably transforming cells with plasmid DNA, Biotechniques 6 (1988) 632–638.

[66] E. Krissinel, K. Henrick, Inference of macromolecular assemblies from crytalline state, J. Mol. Biol. 43 (2007) 774–797.